# Draining of a 2D thin viscous film on a solid particle

Amirhossein Amini

A thesis submitted in partial fulfillment of
the requirements for the degree of

Master of Science in Mechanical Engineering

University of Washington

2012

Reading Committee:

L. N. Brush, Chair

A. Aliseda

T. Duchamp

J. Riley

Program Authorized to Offer Degree:
Mechanical Engineering

University of Washington

**Abstract**

Draining of a 2D thin viscous film on a solid particle

Amirhossein Amini

Chair of the Supervisory Committee:
Professor L. N. Brush
Department of Materials Science & Engineering

In this thesis we derive and solve equations governing the flow of a thin film on a bounded particle with any given geometry, provided it is not cornered or cusped. Our method is to solve the Navier-Stokes, continuity and free surface equations by using asymptotic expansions in powers of the ratio of film thickness to the appropriate length scale of the system using lubrication theory. In the first chapter (1) we describe some of the many industrial processes in which such flows are important, and summarize related work that has been carried out by other authors. In the second chapter (2) the governing lubrication equations and boundary conditions are derived for a simple flat film on an unbounded substrate. The calculations are then extended to a film on a particle using a local normal-tangential coordinate system with independent variables measured by arc length along the solid surface and by the distance normal to the surface. The governing (continuity and Navier-Stokes) equations, the free surface, and no-slip boundary conditions are then rescaled and expanded using lubrication theory in order to derive the final evolution equation for the film thickness (chapter 3). In the fourth chapter (4) particular example of the dynamics of a thin film on an elliptically shaped particle is considered. A MATLAB code is developed to simulate flow dynamics on the elliptical particles. A circle and five different ellipses have been chosen as the solid substrates and the evolution equation has been integrated over each one of them to evaluate the film thickness in time. Finally, we draw our conclusions and suggest further work in the final chapter (5).

## TABLE OF CONTENTS

Page

## LIST OF FIGURES

Figure Number Page

## LIST OF TABLES

Table Number Page

# ACKNOWLEDGMENTS

I am sincerely ever grateful to my advisor, Professor Lucien. N. Brush, who provided excellent guidance and unyielding encouragement throughout all of my endeavors at the University of Washington. I am also very thankful to James Riley for teaching me about fluid mechanics which provided me with invaluable knowledge in pursuit of my research goals, and Professor Thomas Duchamp for helping about many of mathematical aspects in this thesis. This work would not have been possible without the support of department of mechanical engineering in University of Washington. Last, I would like to thank my family and friends for their unwaivering support.

# Chapter 1

# INTRODUCTION

## *1.1 Introduction*

Particles are used as foam and emulsion stabilizing species, with or without surfactant in recent years. Previous work mostly focuses on the effect of particles in emulsion system, but recently the use of particles as foam stabilizers has received great interest, where industries such as flotation and food processing have found the effect of particle stabilization very valuable for many years. Particle contact angle, size and interactions play the major role in stabilization process[1].

Due to the importance of foams and emulsions to many chemical and engineering fields, investigation into the stability, interaction and structural relationships are of great significance. Both liquid and solid foams are practically important to food and beverage industries (e.g. cake and beer), dermatology and personal care industries (e.g. shampoo), textile industries, fire retardants, general polymers/plastics, oil recovery and mineral flotation processing [25]. Emulsions are also heavily used in the food industry, cosmetics and paints, the pharmaceutical industry, agricultural products and the petroleum industry [26].

Although particles are naturally present in many types of emulsions, the use of particles as emulsion stabilizer with or without traditional surfactants, has only been recently studied. There have been a number of different particle types used as stabilizers, including silica, latex particles, metal oxides and sulphates, clays and carbon. The effectiveness of a specific particle type depends on the emulsion medium, the particle shape and size, wettability and inter-particle interaction [20] (In this thesis, the focus is on the effect of the particle shape and size). There is a large size range of particles that can be used to stabilize emulsions.

For successful stabilization, it is necessary that the particles be approximately orders of size smaller than the droplets. The actual size of particles that can be used ranges from small nanometer to micrometer to successfully stabilize emulsions [26]. The size of the particles does correlate to the size of the droplets formed in stable emulsions, with even droplets of up to millimeter having been found stable to coalescence, something not easily possible with surfactants. In general, it can be said that smaller particles produce higher efficiency in stabilization process and as such a more homogeneous layer [20].

As with particles in emulsions, the effect of particle stabilization of foams, has only recently been given attention, which is largely due to successes in emulsions. Yet, it is well known that finely dispersed particles play an important role in the stabilization of many different types of foams. For example, particles in the absence of surfactant are known to cause foaming in rivers, dispersed sludges, distillation towers, oil-well drilling, pulping in the paper industry, fabrication of cellular metal foams and preparation of foods, etc. In the oil industry, obnoxious foams are produced in boilers and various stages of distillation and thought to be stabilized by asphaltene particles [23]. In waste water, foams are stabilized by colloidal particles such as bacteria, soil and viruses. In other cases, heterogeneous nucleation of insoluble precipitates (hydrolysed cations such as iron hydroxides) at the gas/liquid surface can also cause foaming in waste water or rivers. Many other everyday processed products frequently involve particle stabilized foam systems, which ensure long-term stability. In food and drink production (bread and beer have foam like structure) and in the dairy industry when whipping cream, partially crystalline and in the oil droplet accumulate at the interface and stabilize the foam [22].

Understanding the stability and morphological evolution of thin liquid films is vital for a variety of applications such as processing of foam networks, and stabilization of foams and emulsions by using particles. Often the micro and nanoscale physical phenomena in these applications are what determine the resulting bulk scale behavior and properties of the systems [21]. In order to have a precise understanding of the behavior of a wetting or non-wetting 2-D viscous thin film over a solid elliptical particle, it is necessary to be

familiar with topics, such as interfacial fluid dynamics, surface tension, viscosity, and van der Waals forces in general orthogonal coordinates. The next step is to become familiar with lubrication theory. Although intermolecular forces such as van der Waals forces play an important role in the rupture process. In this thesis the results shown will focus on draining and thinning processes, not rupture. The literature review in this section has been sorted in a way that the interested reader could easily follow the materials and build the required background.

### *1.2 Literature Review*

Interfacial fluid dynamics and capillarity have been of interest for almost two centuries. The field was created in the early part of the $19^{th}$ century by Pierre Simon de Laplace (1749-1827) and Thomas Young (1773-1829) [2]. The book Capillarity and Wetting Phenomena [2] has been used in this research in order to understand the surface tension origin and its application to nature and daily life. This book provides a wonderful connection between definitions and mathematical equations, including surface curvature. Later, Henri Bouasse wrote a wonderful account of developments in capillarity in a book he published in 1924. His book enables us to understand the games water can play that help to break monotony of a rainy day or the tricks it performs while washing dishes [3].

The Chapter Interfacial Fluid Dynamics by Stephen H. Davis in perspective in Fluid Dynamics can be used to understand interfacial phenomena and also lubrication theory. It considers the evolution and stability of free films including the effect of van der Waals forces, Marangoni forces, gravity and many others [4].

In 2005, Brush and Davis derived a thinning law for draining flow of a free film between two bubbles. In this thesis, a 2D free-film refers to a liquid film bounded by two gas-liquid interfaces, whereas a thin film refers to a liquid bounded by a solid and a gas liquid interface. This article is very useful for learning how to apply the lubrication theory to a free film problem, which consists of a slightly different mathematic method compare to a film on top of a solid substrate [5]. In their 2008 paper Brush and Roper describe the thinning of lamellae in surfactant-free foams with non-Newtonian liquid phase. This paper includes a complete and clear explanation for free films including the method of matched asymptotic

expansions, which is the main mathematical issue that is involved in the matching process of the flat region (lamellae) with curved borders (Plateau borders). This also can be used in order to become familiar with power-law and Ellis law models of the viscosity[6]. Myers also provides a complete investigation into the use of lubrication models in non-Newtonian thin film flow comparing power-law, Ellis, and Carreau models [7].

The key of dealing with the rupture process is the intermolecular force. Vaynblat, Lister and Witelski examine the van der Waals-driven rupture of a freely suspended thin viscous sheet using long-wavelength models in their 2001 paper. They derive the similarity solutions for both line rupture and point rupture, for unbounded films which leads to an understanding of the dominant forces in the rupture[8]. In 2010 Anderson, Brush and Davis investigated the spontaneous rupture of a thinning free-film due to van der Waals instability in two dimensions. This case is applicable to metallic foams for which surfactants are not available. They describe the thinning process of a liquid film between adjacent bubbles with curved boundaries (Plateau borders) that causes a drainage flow from capillary suction. Linear stability analysis shows that the edge of the film close to the Plateau borders appear more susceptible than the center of the film [9]. More recently McIntyre, Roper and Brush have shown that another mechanism of rupture can appear leading to foam film rupture.

In this thesis, it is desired to handle solid particles with different geometries. In order to deal with this problem, a new coordinate system is used and all of the bulk equations and boundary conditions are written in the new coordinates. Fluid dynamics Theoretical and Computational Approaches [10] has been used as an aid to generate the needed equations and boundary conditions. The approach is more general than those of Howell (1998) who considered a two-dimensional bubble at rest near the surface of a semi-infinite liquid layer. His paper provides a description of the drainage of liquid out of the film under gravity and surface tension using a normal-tangential coordinate system although in this case the lubrication theory only considers free-films that are portions of circular areas. Howell employs a coordinate system that uses the centerline as a reference axis and refers every point in the liquid to the arc-length measured on the centerline, and to a normal distance measured from it [11]. The main difference between his coordinate system and the system used in this thesis is the reference curve. Here it is better to use the solid interface instead of

liquid centerline, since the solid interface is not changing over time. In 1991, Reisfeld and Bankoff investigated the non-isothermal flow of a liquid film on a horizontal cylinder using a similar coordinate system, however, again the circular geometry of the surface makes the coordinate transformation quite simple and as will be shown eliminates some of the very interesting forces deriving flow for the case of non-circular particles. They used lubrication theory to study a thin film under the influence of gravity, capillary, thermocapillary, and intermolecular forces. Their analytical equations and boundary conditions have been used as a special case to check the equations derived in this thesis for a more general case [12]. Finally, to solve the derived evolution equation, analytical tools are no longer useful and it is necessary to use numerical methods for the solution of partial differential equations that are very non-linear and stiff. In 2007 Beerman and Brush used lubrication theory to derive coupled set of strongly nonlinear partial differential equations governing the evolution of interfaces that separate a thin film of pure melt from its crystalline and gas phases. They discretized their equations with backward difference scheme using a quasi-constant step size. Since these nonlinear equations are somewhat mathematically similar to the derived evolution equation in this thesis, their method of discretization is used as the first step towards programming a stable code to solve the evolution equation of the thin film on an elliptical solid substrate[13].

# Chapter 2

# BACKGROUND AND THEORY

## *2.1 Background*

It has been well established that in a thin liquid film on a substrate, fluid flow depends heavily on viscous forces and surface tension. The foundation of thin film analysis is mainly based on interfacial fluid dynamics and lubrication theory.

Problems in interfacial fluid dynamics are intrinsically free-boundary problems. In a free-boundary problem, the shapes, positions and evolution of the boundaries are coupled with the velocity and pressure fields. Therefore, they all must be determined simultaneously [4]. The biggest challenge in handling a free surface problem is hidden in the free boundaries and the most essential role in those boundaries is played by surface tension.

Surface tension plays a major role in numerous scientific endeavors (soil science, climate, plant biology, surface physics, and more), as well as in the chemical industry (product formulation in pharmacology and domestics, the glass industry, automobile manufacturing, textile production, etc.) [2].

Capillarity can be defined as the study of the interfaces between two immiscible liquids or between a liquid and a gas. These interfaces are deformable which allows them to change their shape in response to forces or to minimize surface energy. It is well known that supplying energy is necessary to create surfaces. Suppose one wants to distort a liquid to increase its surface area by an amount $dA$. The work required is proportional to the number of molecules that must be brought to the surface.

$$\delta W = \sigma . dA \tag{2.1}$$

where $\sigma$ is the surface (or interfacial) tension. Dimensionally, $[\sigma]=E\ L^{-2}$ ($E$ is the energy unit and $L$ is unit for length), and surface tension is defined as the energy that must be supplied to increase the surface area by one unit [2]. Due to surface tension, as one passes

across a curved surface or interface, a jump in pressure occurs as evaluated by *Laplace* in the early 19th century.

The increase in hydrostatic pressure $\Delta P$ that occurs when traversing the boundary between two fluids is equal to the product of the surface tension $\sigma$ and the curvature of the surface C.

$$\Delta P = \sigma(\frac{1}{R} + \frac{1}{R'}) = \sigma C \tag{2.2}$$

where $R$ and $R'$ are the radii of curvature of the surface, and $C$ is the mean curvature of the interface.

Intermolecular forces such as van der Waals are essential in the rupture process that happens for films that are sufficiently thin. When the film thickness is less than 200 nms or so, van der Waals attractions or repulsions can extend across the thickness of the film and contribute extra forces beyond those described by Navier-Stokes equations. These forces act to pinch or expand the film at localities where there is a depression in the thickness, depending upon the sign of the forces present[4].

There is currently a big challenge in modeling van der Waals forces; However, the simplest model is from Ruckenstein and Jain [14], in which van der Waals forces are represented as an extra body force $\nabla\phi$ in the Navier-Stokes equation.

$$\rho(\vec{v}_t + \vec{v}.\nabla\vec{v}) = -\nabla p + \mu\nabla^2\vec{v} - \nabla\phi \tag{2.3}$$

For the special case of a film with parallel or quasi-parallel boundaries the van der Waals potential can be written as:

$$\phi = \phi_r + \frac{A}{6\pi h^3} \tag{2.4}$$

Here $\phi_r$ is a reference value, $h$ is the film thickness and $A$ is the Hamaker constant. When $A > 0$, it means that the two interfaces attract each other and the film pinches, alternatively for negative $A$ the interfaces repel[4].

With the knowledge of fluid mechanics equations, surface tension, and van der Waals forces, it is straightforward to generate the bulk equations and boundary conditions for a free

surface problem. The next step is using the lubrication theory to take advantage of the fact that one dimension is much smaller than the other one for thin films, and thereby simplify the derived equations.

Lubrication theory is an appropriate method to investigate fluid motion in thin films. This theory exploits the fact that in the film geometry is significantly smaller in one of the dimensions than the others. The lubrication method helps us find the leading order equations to generate the final evolution equation. The dependent variables are expanded as series in powers of the small film aspect ratio, substituted into the governing equations and interface conditions. This leads to a sequence of problems but for the case at hand, only the leading order problem in the expansion is required. The leading order problem will be used to derive an interface evolution equation.

## 2.2 Theory

### 2.2.1 Interfacial Dynamics

The interface is generally taken to be a mathematical surface of zero thickness separating two phases. It is a free boundary but furthermore, it is the site of localized forces, and is hence an active boundary. If one cuts an interface, there is a force per unit length $\sigma$ acting on the edge; $\sigma$ is the surface or interfacial tension. The interface can, under certain circumstances, exhibit characteristics of surface viscosity and/or elasticity independent of the properties of the bulk fluids. These interfacial forces can create interfacial motions, and, since the bulk fluid is viscous, these motions can be communicated to the bulk. Thus bulk flow can derive the interface, and interfacial flow can derive the bulk; the two are tightly coupled. ( Much of the materials in this Chapter closely follow Davis (1991) [4] )

### 2.2.2 Interfacial Conditions

Consider a system having two bulk phases **I**, **II** separated by an interfacial region $S$. The first boundary condition that will be discussed here is called the kinematic condition. The kinematic condition basically gives the continuity of normal velocity across the interface.
If the bulk velocity field is $\vec{v} = (u, v, w)$ and $V$ is the speed of the interface normal to itself, then the kinematic condition at $S$ can be written as:

$$\vec{v}.\hat{\nu} = V \tag{2.5}$$

where $\hat{\nu}$ is the unit normal vector directed from **II** towards **I**. This convention on the normal vector is important for consistence of the whole process. The intefacial condition in Cartesian coordinate takes the form,

$$w = h_t + uh_x + vh_y \tag{2.6}$$

where $z = h(x, y, t)$.
"It is accepted on empirical grounds that, apart from cases of the flow of rarefied gases and certain instances of moving three-phase lines on solids [15], most viscous fluids have a

continuous tangential velocity. Therefore, on a fluid-fluid interface $S$, the no-slip condition holds,.

$$\vec{v}.\hat{t} = 0 \tag{2.7}$$

where $\hat{t}$ is the unit tangent vector to $S$."

It is necessary to perform a linear momentum balance on the interface to derive two more interfacial conditions. The linear momentum balance in this case includes a force per unit length $\vec{f}_s$ acting on points of the interface. Figure 2.1 shows a control volume in a two dimensional system constructed for the purpose of deriving the additional interface conditions. In general the interface would be endowed with a mass per unit length; in what follows for the sake of simplicity, this is taken to be zero. Here $\vec{\tau_1}$ and $\vec{\tau_2}$ are stress vectors in the bulk fluids acting on areas $S_1$ and $S_2$ respectively. The interface extends from $s$ to $s + \Delta s$ where $s$ is arc-length, and the volume has width $W_0$ normal to the page. Applying Newtons law to the material within $\vartheta = \vartheta_1 + \vartheta_2$ ($\vartheta$ is the total volume), leads to the linear momentum balance in the following form:

(for $i = 1, 2$, $\vec{\tau_i} = \mathbf{T}.\hat{\nu_i}$ where $\nu_i$ are the unit normals.)

$$\frac{d}{dt}\int_{\vartheta} \rho\vec{v}\, d\vartheta = \int_{S_1+S_2} T.\hat{\nu} dS + [\vec{f}_s(s+\Delta s) - \vec{f}_s(s)]W + \int_{\vartheta} \rho\vec{F}\, d\vartheta \tag{2.8}$$

here $\vec{F}$ is the bulk body force per unit mass acting on fluids **I**, **II**, and **T** is the stress tensor. Since the interface mass has been taken to be zero, there is no excess acceleration or body force.

By collapsing the volume $\vartheta$ onto $S$ ($\vartheta \to 0$ and $S_1, S_2 \to S$) (as shown in figure 2.2) $\hat{\nu_1}$ and $\hat{\nu_2}$ becomes $\hat{n}$ and$-\hat{n}$, respectively. Then there is a local balance on $S$:

$$-[T.\hat{n}]W_0\Delta s + [\vec{f}_s(s+\Delta s) - \vec{f}_s(s)]W_0 = 0$$

Dividing by $W_0\Delta s$ and applying the limit $\Delta s \to 0$ gives the point balance equation,

$$-[T.\hat{n}] + \frac{\partial \vec{f}_s}{\partial s} = 0 \tag{2.9}$$

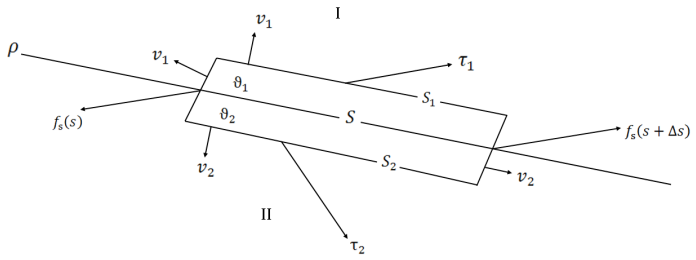


Figure 2.1: Force balance

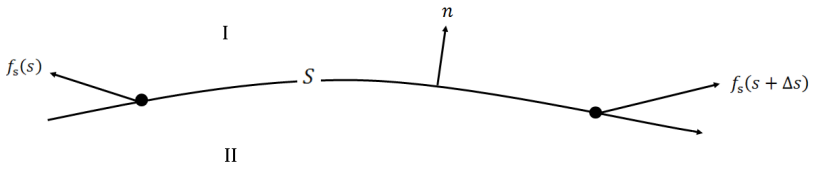


Figure 2.2: Force balance

If there is surface tension $\sigma$ on the interface, then $\vec{f_s} = \sigma\hat{t}$. Applying the Frenet formula given by $\partial\hat{t}/\partial s = \kappa\hat{n}$ ($\kappa = 2H$) where $H$ is the mean curvature of the surface) allows equation 2.9 into the following form,

$$-[T.\hat{n}] + 2H\sigma\hat{n} + \frac{\partial\sigma}{\partial s}\hat{t} = 0. \tag{2.10}$$

The normal component of (2.10) is

$$[\hat{n}.T.\hat{n}] = 2H\sigma \tag{2.11}$$

This boundary condition is also known as the Laplace normal stress balance.
The tangential component of (2.10), which balances the jump in tangential stress with the surface tension gradient, is

$$[\hat{t}.T.\hat{n}] - \frac{\partial\sigma}{\partial s} = 0 \tag{2.12}$$

For constant surface tension equation 2.12 is usually called the no shear stress condition in the literature [4].

### *2.2.3 A thin liquid film on a flat solid substrate*

Now that all the interfacial conditions have been derived, it is useful to study the most basic problem in which there is a thin film evolving on a flat solid substrate [4]. Solving this problem in detail will be illustrative and will provide, basic for working on thin films on solid particles with of different shapes, which is the main subject of this thesis.
Consider a two dimensional thin viscous film on a horizontal substrate as shown in figure 2.3.The mean thickness is $h_0$, gravity is neglected and the liquid has dynamic viscosity $\mu$ and density, $\rho$ both assumed constant. Furthermore, the interface between the liquid and passive gas has a constant surface tension $\sigma$. The problem is solved in Cartesian coordinates with velocity field $\vec{u} = (u, w)$. The solid substrate is stationary and it is located at $z = 0$, and the gas/liquid interface is at $z = h(x, t)$. The governing equations in the bulk fluid are Stokes equations for viscous flow since the Reynolds number is very small in the high aspect ratio film geometry.

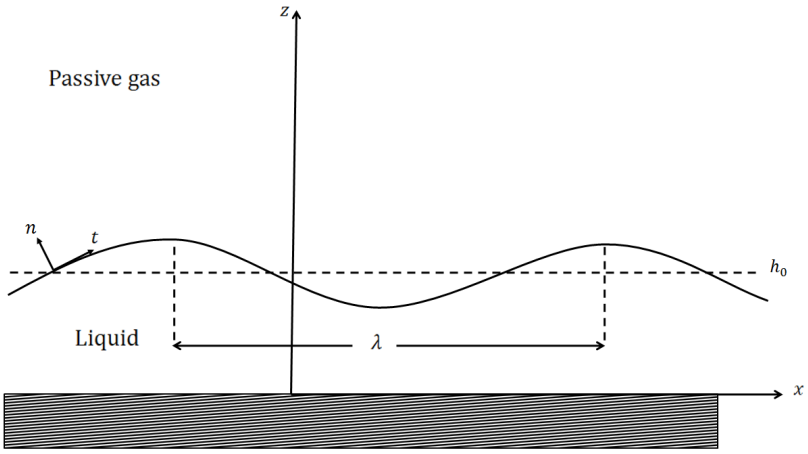


Figure 2.3: Thin film on a solid substrate

$$\rho(u_t + uu_x + wu_z) = -p_x + \mu(u_{xx} + u_{zz}) \tag{2.13}$$

$$\rho(w_t + uw_x + ww_z) = -p_z + \mu(w_{xx} + w_{zz}) \tag{2.14}$$

and continuity for incompressible liquids

$$u_x + w_z = 0 \tag{2.15}$$

There are the a no-slip and the no penetration boundary conditions at the solid/liquid interface ($z = 0$)

$$u = w = 0 \tag{2.16}$$

The kinematic condition (2.5) at $z = h(x, t)$ is

$$w = h_t + uh_x \tag{2.17}$$

The conditions on the tangential and normal components of the stress(2.12 and 2.11) require evaluation of the components of the stress tensor:

$$T_{xx} = -p + 2\mu u_x \qquad T_{xy} = \mu(u_z + w_x) = T_{yx} \qquad T_{yy} = -p + 2\mu w_z \ .$$

Identifying the normal and tangential unit vectors as

$$\hat{n} = \frac{1}{n}(-h_x, 1) \qquad \hat{t} = \frac{1}{n}(1, h_x) \qquad n = (1 + h_x^2)^{1/2}$$

then the condition on the tangential component of the stress tensor at the interface is:

$$[\hat{t}.T.\hat{n}] = 0(u_z + w_x)(1 - h_x^2) - 4h_x u_x = 0 \ . \tag{2.18}$$

and the normal stress balance is written:

$$[\hat{n}.T.\hat{n}] = 2H\sigma \quad \Rightarrow \quad -p + 2\mu[w_z(1 - h_x^2) - h_x(u_z + w_x)]/n^2 = 2H\sigma \tag{2.19}$$

where

$$2H = h_{xx}/n^3 \tag{2.20}$$

and the continuity equation (2.15) has been applied. In order to simplify the system and gain an understanding of the dynamics of the interface, it is useful to carry out a dimensional analysis on the system. The horizontal length scale has been chosen as $L$ and the vertical as $h_0$. The velocity scale in the x-direction is taken to be $U_0$. Continuity (2.15) makes the other velocity scale $W_0 = \epsilon U_0$, where $\epsilon$ is $(h_0/L)$. An appropriate time scale for this problem is $T_0 = L/U_0$.

The non-dimensional form of governing equations and boundary conditions using aforementioned scales is:

$$U_X + W_Z = 0 \tag{2.21}$$

$$\epsilon Re(U_T + UU_X + WU_Z) = -P_X + U_{ZZ} + \epsilon^2 U_{XX} \tag{2.22}$$

$$\epsilon^3 Re(W_T + UW_X + WW_Z) = -P_Z + \epsilon^2(W_{ZZ} + \epsilon^2 W_{XX}) \tag{2.23}$$

at $Z = 0$

$$U = W = 0 \tag{2.24}$$

at $Z = H$

$$W = H_T + UH_X \tag{2.25}$$

$$(1-\epsilon^2)(U_Z + \epsilon^2 W_X) - 4\epsilon^2 H_X U_X = 0 \tag{2.26}$$

$$-P + 2\epsilon^2[W_Z(1-\epsilon^2 H_X^2) - H_X(U_Z + \epsilon^2 W_X)]/n^2 = Ca^{-1}\epsilon^3 H_{XX}/n^3 \tag{2.27}$$

Here the pressure scale is $P_0 = \mu U_0/(\epsilon h_0)$, which is chosen to balance pressure and viscous forces. The dimensionless parameters are the capillary number ($Ca$) and length ratio ($\epsilon$).

$$Ca = \frac{U_0\mu}{\sigma} \qquad \epsilon = \frac{h_0}{L} \tag{2.28}$$

The dependent variables are extended in series, $(U, W, P) = (U_0, W_0, P_0) + \epsilon(U_1, W_1, P_1) + \cdots$ and substituted into governing equations and boundary conditions generating a sequence of problems in increasing powers of $\epsilon$. The leading order system in this approximation is all that is required to solve this problem and is the lubrication approximation, which applies to solutions with slow variations in $x$ and $t$. Note from the boundary condition (2.27) that as $\epsilon \to 0$, if $Ca = O(1)$, then the surface tension is lost from the lubrication theory. It turns out that ignoring surface tension makes various problems ill-posed; the growth rate of instabilities become unbounded as the wavenumber approaches infinity and the neglect of surface tension does not correspond to the physical situation at hand because surface tension is known to play a role in the film dynamics. Thus, one wishes to retain surface tension and so takes $Ca^{-1}\epsilon^3 = O(1)$ by defining

$$\tilde{C}^{-1} = \epsilon^3 Ca^{-1} \tag{2.29}$$

so that surface tension $\sigma$ is large, $\sigma \sim \epsilon^{-3}$.

It can be said that an important step in dealing with many free surface problems is picking the right order of capillary number in order to balance dominant forces. The appropriate order of $Ca$ varies for different problems depending on type of boundaries and it strongly

affects the evolution equation. For example although a film on a solid substrate requires $Ca \sim O(\epsilon^3)$, the proper scaling of surface tension for a free film is $Ca \sim O(\epsilon)$.
Substituting the series into the governing dimensionless system, gives the $O(1)$ problem:

$$U_{ZZ} = P_X \qquad P_Z = 0 \qquad U_X + W_Z = 0 \tag{2.30}$$

at $Z = 0$

$$U = 0 \qquad W = 0 \tag{2.31}$$

at $Z = H$

$$W = H_T + UH_X \qquad U_Z = 0 \qquad -P = \tilde{C}^{-1} H_{XX} \tag{2.32}$$

The leading order Stokes equation in z-direction (2.30) illustrates the fact that the pressure profile is independent of $z$. The pressure profile can be determined everywhere, considering that $P = P(X,T)$ and using the leading order form of the Laplace normal stress boundary condition (2.32),

$$P = P(X,T)$$

$$P_{|_{Z=H}} = P(X,T)$$

$$P(X,T) = -\tilde{C}^{-1} H_{XX} \tag{2.33}$$

and the axial component of the motion equation may be integrated to find,

$$U_Z = \frac{\partial P}{\partial X} Z + f(X,T)$$

and the axial component of stress balance indicates that,

$$f(X,T) = -\frac{\partial P}{\partial X} H \tag{2.34}$$

Integrating once more gives:

$$U = \frac{\partial P}{\partial X} \frac{Z^2}{2} + f(X,T)Z + g(X,T)$$

where $g(X,T)$ must be zero to satisfy the no-slip condition.

$$U = \frac{\partial P}{\partial X}(\frac{Z^2}{2} - HZ) \tag{2.35}$$

Integrating continuity gives:

$$\int_0^H U_X \, dZ + W_{|_{Z=H}} - W_{|_{Z=0}} = 0$$

where $W = 0$ at $z = 0$. Using the kinematic condition leads to:

$$\int_0^H U_X \, dZ = -W_{|_{Z=H}} = -(H_T + U_{|_{Z=H}} H_X)$$

on the other hand, by using Leibniz integral rule:

$$\int_0^H U_X \, dZ = \frac{\partial}{\partial X}\int_0^H U \, dZ - H_X U_{|_{Z=H}} = -H_T - U_{|_{Z=H}} H_X \Longrightarrow \frac{\partial}{\partial X}\int_0^H U \, dZ + H_T = 0$$

The evolution equation can be derived from above equation, since the pressure (2.33) and velocity profile (2.35) have been evaluated,

$$3H_T + \tilde{C}^{-1}(H_{XXX}H^3)_X = 0 \tag{2.36}$$

Equation 2.36 is an evolution equation for $H$ in time. This is valid for films larger than 1000 Angstroms where van der Waals forces may be neglected.

The same method can be applied generally to a thin film on a solid substrate with different geometry, but the governing equations and boundary conditions need to be developed in general coordinates. This procedure will be fully explained in the next chapter.

# Chapter 3

# THIN FILMS ON SOLID SUBSTRATES WITH DIFFERENT GEOMETRIES

The goal of this chapter is to derive bulk equations and boundary conditions for a 2-D viscous thin film with constant surface tension on a stationary solid particle. The analysis that is used in this chapter can be applied to solid particles of any shape (circular, elliptical, flat, etc.). In order to handle particles with different geometries it is necessary to pick the right coordinate system. The next step is to develop needed equations and boundary conditions in the chosen coordinate system. To gain a better understanding of the dynamics of the film, it is helpful to apply dimensional analysis that will identify the appropriate dimensionless numbers for the system. The main dimensionless number in this problem is expected to be the capillary number since surface tension and viscous forces are the two dominant forces. The final step towards deriving an evolution equation is applying lubrication theory on the system using a regular perturbation in $\epsilon$, the ratio of film thickness to the proper length scale. This process will lead us to the appropriate leading order equations and boundary conditions, modelling the evolution equation of the film interface.

### *3.1 Coordinate System*

The appropriate coordinate system must be able to handle different geometries since there is no assumption made about particle shape in this chapter (except that it is not cornered or cusp). The appropriate choice will ease the evaluation of free surface boundary conditions (2.11, 2.12). Based on this criteria and on previous work in this field, the best choice is coordinate system that is defined by the normal and tangential direction of the solid/liquid interface. In his 1998 paper, Howell considers a two-dimensional bubble at rest near the surface of a semi-infinite liquid layer. His choice of coordinate system, uses the centerline as the reference coordinate curve in which every point in the liquid of the film is measured with respect to arc-length along the centerline and normal distance measured from it. For this work, it is better to use the solid interface instead of the liquid-film centerline as the reference curve, since the solid interface is not changing over time.

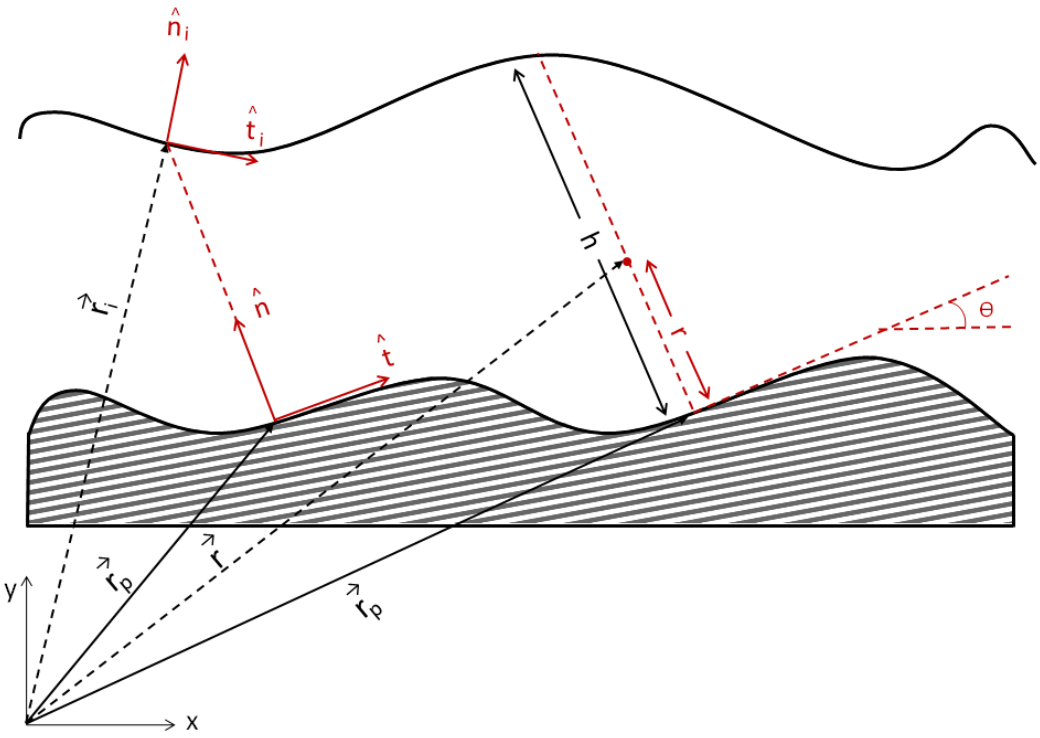


Figure 3.1: Normal Tangential Coordinate System

The orthogonal normal-tangential local coordinates are used to address any point in the bulk fluid or on the interface (3.1). The bottom edge, which is the solid/liquid interface, was chosen as the reference curve. The reference curve arc-length **s** and the normal distance from the bottom **r** are the two independent variables in this coordinate system. Each point on the bottom interface can be addressed by a specific arc-length, measured on itself, in other words, the solid/liquid interface is the $r = 0$ curve. Any point in the bulk fluid is addressed by an arc-length measured on the reference curve **s** and a normal distance from it **r**. To gain a better understanding of the coordinate system and its derivatives it is useful to consider $s$-constant and $r$-constant curves. As shown in figure 3.2, the $r$ constant curves are parallel to the solid edge with the distance $r$. The partial derivative with respect to $s$ of any parameter simply measures change along one of these parallel curves. The $s$-constant coordinate lines are normal to the solid interface. Along $s$-constant contours both normal

and tangential vectors remain constant. In general the gas/liquid interface does not align with a constant $r$-coordinate contour and therefore, the normal and tangential vectors on free surface can be different from those in the bulk liquid with the same $s$ (Figure 3.2).

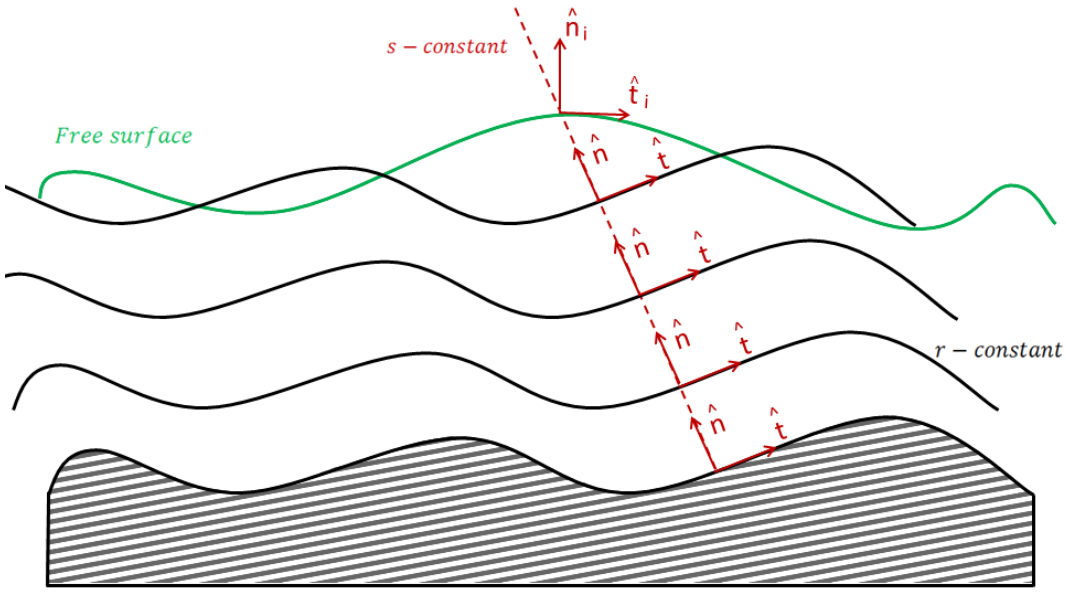


Figure 3.2: r-constant and s-constant curves

Consider a 2-D system consisting of a liquid film on top of a solid as shown in figure 3.1. The solid/liquid interface is parameterized by $\vec{r}_p(s)$ in the inertial reference frame. Since the solid/liquid interface of a stationary particle is not changing during time, $\vec{r}_p$ is not a function of time, i.e.

$$\vec{r}_p(s) = x_p(s)\hat{i} + y_p(s)\hat{j} \tag{3.1}$$

where $\hat{i}$ and $\hat{j}$ are the Cartesian unit vectors.

Any point in the bulk liquid is a function of $s$ (the arc-length measured on the reference curve) and $r$ ( the normal distance from the solid/liquid interface), and is written:

$$\vec{r}(r, s, t) = \vec{r}_p(s) + r\hat{n}(s) \tag{3.2}$$

($\hat{n}$ is the unit normal to the bottom interface). In Cartesian coordinates

$$\vec{r}(r, s, t) = (x_p(s) - r\sin\theta)\hat{i} + (y_p(s) + r\cos\theta)\hat{j} \tag{3.3}$$

where $\theta$ is the angle between the tangent line and the horizon.
By using arc-length calculations it is straightforward to evaluate the normal and tangential unit vectors on any point of bottom interface. Recall that unit vectors stay the same among a $s$-constant line up to the top interface (figure 3.2), thus

$$\frac{dx_p}{ds} = \cos\theta \qquad \frac{dy_p}{ds} = \sin\theta$$

$$\frac{\partial\vec{r}_p}{\partial s} = \cos\theta\hat{i} + \sin\theta\hat{j} \Longrightarrow |\frac{\partial\vec{r}_p}{\partial s}| = 1$$

$$\hat{t} = \cos\theta\hat{i} + \sin\theta\hat{j} \qquad \hat{n} = -\sin\theta\hat{i} + \cos\theta\hat{j} \tag{3.4}$$

The top interface in these coordinates is denoted by $\vec{r}_i$, and derived by substituting $r$ with $h(s, t)$ in equation 3.2, where $h$ is the thickness of the film measured normal to the particle surface . As shown below, the top interface is only function of arc-length and time.

$$\vec{r}_i(s,t) = \vec{r}_p(s) + h(s,t)\hat{n}(s) \tag{3.5}$$

Normal and tangential unit vectors of the top interface $(n_i, t_i)$ are needed to evaluate the free surface boundary conditions (2.11 and 2.12). Figure 3.2 shows that the unit vectors on the top interface are different from those in the bulk fluid. These unit vectors can be evaluated using the Frenet formula:

$$\frac{d\hat{t}}{ds} = \theta_s \hat{n} \qquad \frac{d\hat{n}}{ds} = -\theta_s \hat{t}$$

where $\theta_s$ is the curvature of solid/liquid interface. Therefore

$$\frac{\partial \vec{r}_i}{\partial s} = \frac{\partial \vec{r}_p}{\partial s} + h_s\hat{n} - h\theta_s\hat{t} = (1 - h\theta_s)\hat{t} + h_s\hat{n}$$

where

$$N = (h_s^2 + (1 - h\theta_s)^2)^{1/2}$$

It follows that

$$\hat{t}_i = \frac{1}{N}\{(1 - h\theta_s)\hat{t} + h_s\hat{n}\} \tag{3.6}$$

$$\hat{n}_i = \frac{1}{N}\{-h_s\hat{t} + (1 - h\theta_s)\hat{n}\} \tag{3.7}$$

The sufficient condition for this coordinate system to address each point uniquely is that the film thickness is smaller than the minimum radius of curvature of the bottom interface. Figure 3.4 shows that when this condition is not satisfied there could be a point addressed from two (or more) different points on the reference curve $r = 0$. (Figure 3.3).

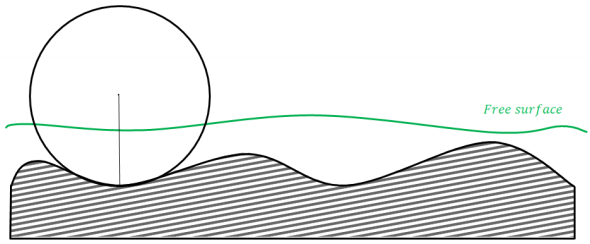


Figure 3.3: Thickness<Minumum Radius of Curvature

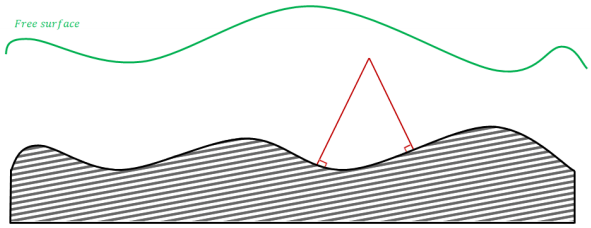


Figure 3.4: Thickness>Minumum Radius of Curvature

### *3.2 Fluid Mechanics Governing Equations*

In this section governing fluid mechanic equations are developed for a 2-D thin film on a solid stationary substrate. The surface tension is taken to be constant and gravity is neglected. The liquid is viscous enough to assume the Reynolds number is very small and Stokes flow is appropriate. Fluid mechanic equations in general coordinates are presented in reference [10]. The bulk fluid is assumed to be incompressible and the bulk fluid velocity

is taken to be:

$$\vec{u} = u\hat{t} + v\hat{n} \tag{3.8}$$

where $\hat{t}$ and $\hat{n}$ are the vectors illustrated in Figure (3.1). The 2-D conservation of mass in general coordinates can be written as below:

$$\nabla \cdot \vec{u} = \frac{1}{h_1 h_2}\{\frac{\partial}{\partial \xi_1}(h_2 u) + \frac{\partial}{\partial \xi_2}(h_1 v)\} = 0 \tag{3.9}$$

where $\xi_1$ and $\xi_2$ are the independet variables ($s$,$r$) and $h_1$ and $h_2$ are:

$$h_1 = 1 - r\theta_s \qquad h_2 = 1 \ . \tag{3.10}$$

The continuity equation for our coordinate system is derived combining 3.9 and 3.10 with independent variables $s$ and $r$,

$$u_s - v\theta_s + (1 - r\theta_s)v_r = 0 \ . \tag{3.11}$$

A similar process is used to derive the Stokes equation ($-\nabla P + \mu\nabla^2\vec{u} = 0$). In general coordinates these equations are:

$$\frac{1}{h_1^2 h_2}\{\frac{\partial}{\partial \xi_1}(h_1 h_2 T_{\xi_1\xi_1}) + \frac{\partial}{\partial \xi_2}(h_1^2 T_{\xi_1\xi_2})\} - \frac{1}{h_1^2}\frac{\partial h_1}{\partial \xi_1}T_{\xi_1\xi_1} - \frac{1}{h_1 h_2}\frac{\partial h_2}{\partial \xi_1}T_{\xi_2\xi_2} = 0 \tag{3.12}$$

$$\frac{1}{h_1 h_2^2}\{\frac{\partial}{\partial \xi_1}(h_2^2 T_{\xi_1\xi_2}) + \frac{\partial}{\partial \xi_2}(h_1 h_2 T_{\xi_2\xi_2})\} - \frac{1}{h_1 h_2}\frac{\partial h_1}{\partial \xi_2}T_{\xi_1\xi_1} - \frac{1}{h_2^2}\frac{\partial h_2}{\partial \xi_2}T_{\xi_2\xi_2} = 0 \tag{3.13}$$

where stress tensor components for incompressible liquids are:

$$T_{\xi_1\xi_1} = -p + 2\mu(\frac{1}{h_1}\frac{\partial u}{\partial \xi_1} + \frac{v}{h_1 h_2}\frac{\partial h_1}{\partial \xi_2}) \ , \tag{3.14}$$

$$T_{\xi_2\xi_2} = -p + 2\mu(\frac{1}{h_2}\frac{\partial v}{\partial \xi_2} + \frac{u}{h_1 h_2}\frac{\partial h_2}{\partial \xi_1}) \ , \tag{3.15}$$

and

$$T_{\xi_1\xi_2} = \mu(\frac{1}{h_1}\frac{\partial v}{\partial \xi_1} + \frac{1}{h_2}\frac{\partial u}{\partial \xi_2} - \frac{v}{h_1 h_2}\frac{\partial h_2}{\partial \xi_1}) \tag{3.16}$$

Evaluating this for our case gives:

$$T_{ss} = -p - 2\mu v_r \ , \tag{3.17}$$

$$T_{sr} = \frac{\mu}{1 - r\theta_s}(v_s + (1 - r\theta_s)u_r + u\theta_s) \ , \tag{3.18}$$

and

$$T_{rr} = -p + 2\mu v_r \tag{3.19}$$

The components of the viscous flow equations in normal-tangential coordinate system are:

$$-\frac{\partial}{\partial s}(p+2\mu v_r)+\frac{\partial}{\partial r}\{\mu(v_s+(1-r\theta_s)u_r+u\theta_s)\}-\frac{\mu\theta_s}{1-r\theta_s}(v_s+(1-r\theta_s)u_r+u\theta_s)=0 \tag{3.20}$$

(axial balance)

and

$$\frac{\partial}{\partial s}\{\frac{\mu}{1 - r\theta_s}(v_s + (1 - r\theta_s)u_r + u\theta_s)\} - 4\mu v_r\theta_s + (1 - r\theta_s)\frac{\partial}{\partial r}(-p + 2\mu v_r) = 0 \tag{3.21}$$

(transverse balance)

### *3.3 Boundary Conditions*

As mentioned in chapter 2, this free surface problem includes five different boundary conditions. There are the no-slip and no penetration conditions satisfied on the bottom interface, as well as the kinematic condition (2.5), and tangential (2.10) and the normal stress balance (2.11) conditions at the liquid/gas interface.

the no-slip and no penetration condition on the bottom interface for the stationary particle are:

$$u|_{r=0} = 0, \qquad v|_{r=0} = 0 \tag{3.22}$$

The kinematic condition in this coordinate system is [16]:

$$v|_{r=h} = h_t + \frac{h_s u}{1 - h\theta_s} \tag{3.23}$$

The tangential component of the stress balance is:

$$4(1 - h\theta_s)h_s v_r + \frac{1}{1 - h\theta_s}(v_s + (1 - h\theta_s)u_r + u\theta_s)\{(1 - h\theta_s)^2 - h_s^2\} = 0 \tag{3.24}$$

The normal component of stress balance is:

$$\begin{aligned} &-p + \{-2\mu h_s(v_s + (1 - h\theta_s)u_r + u\theta_s) + 2\mu v_r(-h_s^2 + (1 - h\theta_s)^2)\}/N^2 \\ &= \sigma\{\theta_s(1 - h\theta_s)^2 + h_{ss}(1 - h\theta_s) + 2h_s^2\theta_s + hh_s\theta_{ss}\}/N^3 \end{aligned} \tag{3.25}$$

To ensure robust results the curvature of interface ($k_i$) was calculated by three different methods. The curvature calculated by all three methods is,

$$k_i = \frac{(\theta_s(1 - h\theta_s)^2 + h_{ss}(1 - h\theta_s) + 2h_s^2\theta_s + hh_s\theta_{ss})}{\{(1 - h\theta_s)^2 + h_s^2\}^{3/2}} \tag{3.26}$$

These calculations are fully explained in Appendix A.

### *3.4 Summary of Governing Equations and Boundary Conditions*

In the bulk film:

$$u_s - v\theta_s + (1 - r\theta_s)v_r = 0 \tag{3.27}$$

$$-\frac{\partial}{\partial s}(p + 2\mu v_r) + \frac{\partial}{\partial r}\{\mu(v_s + (1 - r\theta_s)u_r + u\theta_s)\} - \frac{\mu\theta_s}{1 - r\theta_s}(v_s + (1 - r\theta_s)u_r + u\theta_s) = 0 \tag{3.28}$$

$$\frac{\partial}{\partial s}\{\frac{\mu}{1-r\theta_s}(v_s+(1-r\theta_s)u_r+u\theta_s)\}-4\mu v_r\theta_s+(1-r\theta_s)\frac{\partial}{\partial r}(-p+2\mu v_r)=0 \tag{3.29}$$

at $r=0$

$$u|_{r=0}=0 \qquad v|_{r=0}=0 \tag{3.30}$$

at $r=h(s,t)$

$$v|_{r=h}=h_t+\frac{h_s u}{1-h\theta_s} \tag{3.31}$$

$$4(1-h\theta_s)h_s v_r+\frac{1}{1-h\theta_s}(v_s+(1-h\theta_s)u_r+u\theta_s)\{(1-h\theta_s)^2-h_s^2\}=0 \tag{3.32}$$

$$\begin{aligned}-p+\{-2\mu h_s(v_s+(1-h\theta_s)u_r+u\theta_s)+2\mu v_r(-h_s^2+(1-h\theta_s)^2)\}/N^2\\ =\sigma\{\theta_s(1-h\theta_s)^2+h_{ss}(1-h\theta_s)+2h_s^2\theta_s+hh_s\theta_{ss}\}/N^3\end{aligned} \tag{3.33}$$

### *3.5 Dimensional Analysis and Lubrication Theory*

In order to gain a better understanding of the system and, to apply lubrication theory, dimensional analysis is necessary. This process simplifies the equations and illustrates the correct dimensionless numbers. The length scale for the lateral arc-length coordinate is chosen to be the minimum radius of curvature ($L=R_{min}=1/k_{max}$). The film thickness has been scaled by $h_0$, which is the average film thickness. Tangential velocity is scaled by $u_0$ and the normal velocity by $v_0$, where $v_0 \ll u_0$. The kinematic boundary condition can be used to determine the appropriate time scale for the problem, which is $T_0=L_0/U_0$. The pressure is chosen to balance viscous forces leading to the pressure scale factor $P_0=\mu u_0/(h_0\epsilon)$, which is the same pressure scale as flat case that has been explained in Chapter 2. Scales are shown in table 3.1.

Table 3.1: Scales Definition

| Scaling | Var descrip | Scale Descrip |
|---|---|---|
| $S = s/L$ | Arc-length | Minimum Radius of curvature |
| $R = r/h_0$ | Normal distance | Average thickness |
| $H = h/h_0$ | Film thickness | Average thickness |
| $K = Lk$ | Curvature of reference curve | $k_{max}$ |
| $U = u/u_0$ | Tangential velocity | - |
| $V = v/v_0$ | Normal velocity | - |
| $P = p/P_0$ | Pressure | $P_0 = \mu u_0/(h_0\epsilon)$ |
| $T = t/T_0$ | Time | $T_0 = L_0/U_0$ |

The capillary number $Ca$, and length ratio $\epsilon$ are two dimensionless numbers remaining.

$$Ca = \frac{U_0\mu}{\sigma} \qquad \epsilon = \frac{h_0}{L} \tag{3.34}$$

The dimensionless form of the model is given below,

The continuity equation is:

$$U_S - \epsilon V K + (1 - \epsilon R K)V_R = 0 \tag{3.35}$$

The equation of motion in the longitudinal direction is:

$$-\frac{\partial}{\partial S}(P+2\epsilon^2 V_R)+\frac{\partial}{\partial R}\{(\epsilon^2 V_S+(1-\epsilon RK)U_R+\epsilon UK)\}-\frac{K}{1-\epsilon RK}(\epsilon^3 V_S+\epsilon(1-RK)U_R+\epsilon^2 UK)=0\ , \tag{3.36}$$

and in the transverse direction is:

$$\frac{\partial}{\partial S}\{\frac{\epsilon}{1-\epsilon RK}(\epsilon^3 V_S+\epsilon(1-\epsilon RK)U_R+\epsilon^2 UK)\}-4\epsilon^3 V_R K+(1-\epsilon RK)\frac{\partial}{\partial R}(-P+2\epsilon^2 V_R)=0 \tag{3.37}$$

The no-slip and no-penetration conditions are:

$$U|_{R=0}=0\ \ ,\ \ V|_{R=0}=0 \tag{3.38}$$

The kinematic condition is:

$$t_o=\frac{h_o}{v_o}$$
$$V|_{R=H}=H_T+\frac{H_S U|_{R=H}}{1-\epsilon HK} \tag{3.39}$$

The tangential component of the stress tensor obeys:

$$4\epsilon^2(1-\epsilon HK)H_S V_R+\frac{1}{1-\epsilon HK}(\epsilon^2 V_S+(1-\epsilon HK)U_R+\epsilon UK)\{(1-\epsilon HK)^2-\epsilon^2 H_S^2\}=0\ , \tag{3.40}$$

and the normal component obeys:

$$-\frac{CaP}{\epsilon}+\{-2CaH_S(\epsilon^3 V_S+(1-\epsilon HK)U_R+\epsilon UK)+2CaV_R(-\epsilon^2 H_S^2+(1-\epsilon HK)^2\}/N_\epsilon^2$$

$$= \{\epsilon K(1-\epsilon HK)^2 + \epsilon^2(1-\epsilon HK)H_{SS} + 2\epsilon^3 H_S^2 K + \epsilon^3 H H_S K_{SS}\}/N_\epsilon^3 \tag{3.41}$$

where,

$$N_\epsilon = (\epsilon^2 H_S^2 + (1-\epsilon HK)^2)^{0.5} \tag{3.42}$$

### *3.6 Lubrication Theory*

Approximate solutions are developed, using regular perturbation theory. At fixed capillary number the dependent variables are expanded in powers of $\epsilon$, $(U, V, P) = (U_0, V_0, P_0) + \epsilon(U_1, V_1, P_1) + \cdots$. This leads to a sequence of problems at increasing orders in $\epsilon$.
At leading order the system becomes,

$$U_S + V_R = 0 \tag{3.43}$$

$$-P_S + U_{RR} = 0 \tag{3.44}$$

$$P_R = 0 \tag{3.45}$$

$$U|_{R=0} = V|_{R=0} = 0 \tag{3.46}$$

$$V|_{R=H} = H_T + U|_{R=H} H_S \tag{3.47}$$

$$U_R = 0 \tag{3.48}$$

For the normal component of the stress tensor the full dependence of $\epsilon$ is retained for the discussion that follows,

$$-P+\epsilon\{-2H_S(\epsilon^3V_S+(1-\epsilon HK)U_R+\epsilon UK)+2V_R(-\epsilon^2H_S^2+(1-\epsilon HK)^2\}/N_\epsilon^2$$
$$=\epsilon Ca^{-1}\{\epsilon K(1-\epsilon HK)^2+\epsilon^2(1-\epsilon HK)H_{SS}+2\epsilon^3H_S^2K+\epsilon^3HH_SK_{SS}\}/N_\epsilon^3 \quad (3.49)$$

Note that from the normal stress condition (3.49) as $\epsilon \to 0$, if $Ca = O(1)$ then the surface tension is lost from the lubrication theory. Ignoring surface tension makes various problems ill-posed: for example the growth rate of an instability becomes unbounded as the wavenumber approaches infinity. Therefore, to retain surface tension requires $Ca^{-1}\epsilon^3 = O(1)$, which is achieved by defining,

$$\tilde{C}^{-1} = \epsilon^3 Ca^{-1} \quad \sim o(1) \quad (3.50)$$

and substitute the result into 3.49. This substitution requires the surface tension $\sigma$ to be large: $\sigma \sim \epsilon^{-3}$. Finally, by using 3.50 the leading order interface boundary condition is now written as:

$$-P = \tilde{C}^{-1}\{\frac{K}{\epsilon} - 2HK + H_{SS}\} \quad (3.51)$$

The governing equations and boundary conditions can be compared with the work of B. Reisfeld & S. G. Bankoff [12], who examined the behavior of film on circular substrate. The polar coordinate system can be assumed as a special case of the general normal-tangential coordinate system considered here.

Equation 3.51 admits different scaling limits. When $K$ is $O(1)$, the $K/\epsilon$ term becomes the dominant term on the right hand side (3.52),

$$K \sim O(1)$$

and

$$-P = \tilde{C}^{-1}K \quad (3.52)$$

On the other hand, if $K \sim O(\epsilon)$ then

$$\tilde{K} = K\epsilon^{-1} \sim O(1)$$

and

$$-P = \tilde{C}^{-1}(\tilde{K} + H_{SS}) \tag{3.53}$$

As will be shown these two limits lead to different equations for the film thickness.

### *3.7 Evolution Equations*

For thin-film on a solid particle we only need to solve the leading order equations and conditions. Two different evolution equations are derived, depending on the order of the dimensionless solid/liquid interface curvature.

Eqn. 3.64 shows that the profile is independent of $R$.

$$P = P(S,T)$$

Eqn. 3.54 gives the pressure

$$P(S,T) = -\tilde{C}^{-1}K \tag{3.54}$$

if the particle curvature $K \sim O(1)$.

As shown in equation 3.54 the pressure profile in this case is independet of the film thickness.

If the particle curvature is order $\epsilon$ then:

$$P(S,T) = -\tilde{C}^{-1}(\tilde{K} + H_{SS}) \tag{3.55}$$

where in equation 3.55, $\tilde{K} = K\epsilon^{-1}$. Eqn. 3.63 may be integrated to find,

$$U_R = \frac{\partial P}{\partial S}R + f(S,T)$$

and the condition 3.67 is used to evaluate,

$$f(S,T) = -\frac{\partial P}{\partial S}H$$

Integrating once more gives:

$$U = \frac{\partial P}{\partial S}\frac{R^2}{2} + f(S,T)Z + g(S,T)$$

and the no-slip condition (3.22) requires:

$$g(S,T) = 0$$

Therefore the tangential component of the fluid velocity is:

$$U = \frac{\partial P}{\partial S}(\frac{R^2}{2} - HR) \tag{3.56}$$

Integrating the continuity (3.62) over the film thickness gives

$$\int_0^H U_S\, dR + V_{|_{R=H}} - V_{|_{R=0}} = 0$$

where $V = 0$ at $R = 0$, so that

$$\int_0^H U_S\, dR = -V_{|_{R=H}} = -(H_T + U_{|_{R=H}} H_S)$$

By using the Leibniz integral rule:

$$\int_0^H U_S\, dR = \frac{\partial}{\partial S}\int_0^H U\, dR - H_S U_{|_{R=H}} = -H_T - U_{|_{R=H}} H_S \Longrightarrow \frac{\partial}{\partial S}\int_0^H U\, dR + H_T = 0$$

The evolution equation can be derived from above equation, since the pressure (**??** or 3.55) and velocity profile (3.56) have been evaluated,

Case **I**: $K \sim O(\epsilon)$

$$3H_T + \frac{\partial}{\partial S}\{(\tilde{C}^{-1}(\tilde{K}_S + H_{SSS})H^3\} = 0 \tag{3.57}$$

Case **II**: $K \sim O(1)$

$$3H_T + \frac{\partial}{\partial S}\{\tilde{C}^{-1}K_S H^3\} = 0 \tag{3.58}$$

Equations 3.57 and 3.58 are evolution equations for H. These two partial differential equations do not govern rupture processes, which occur when a film is thin enough (less than 1000 angstroms). In order to find the governing evolution equation for rupture, van der Waals forces must be considered as a body force in the bulk fluid equations.

### *3.8 Intermolecular Forces*

The molecules in a film interact with themselves and with the neighboring gas or substrate. However, when a film has a thickness in the range 100-1000 Angstroms van der Waals attractions or repulsion can extend across the thickness of the film and contribute significant additional forces beyond those described by the Navier-Stokes equations [4].

In this section van der Waals forces have been added to system that has been studied previously in this chapter. Gravity is neglected and the surface tension is assumed to be constant everywhere. The fluid is chosen to be viscous enough to allow the neglect inertia. The van der Waals potential has been added to the Stokes equations as a body force in the form:

$$-\nabla p + \mu\nabla^2\vec{u} - \nabla\phi = 0 \tag{3.59}$$

where

$$\phi = \phi_r + \frac{\bar{A}}{\bar{h}^3} + \frac{\bar{B}}{\bar{h}^n} \tag{3.60}$$

where $\phi_r$ is a reference constant, A is the Hamaker constant and the latter term $B/h^n$ represents a repulsive force. Strictly speaking Eqn. (3.61) is valid for uniform films with flat interfaces and a constant thickness $\bar{h}$. The difference between $h$ and $\bar{h}$ is shown in figure 3.5. However, in this research, even though the interfaces are slightly non-parallel in real space, this expression will be used to represent the intermolecular forces. Here the distance $\bar{h}$ will be given by the distance $h$ from the particle surface to the gas/liquid interface along its normal (fixed $S$). This is a leading order approximation to the intermolecular forces and is consistent with the longwave theory. Therefore,

$$\phi = \phi_r + \frac{\bar{A}}{h^3} + \frac{\bar{B}}{h^4} \tag{3.61}$$

Defining an effective pressure $p^*$ easily allows us to adjust all the derived equations in sections 3.2-3.6. Using $p^*=p+\phi$, the adjusted leading order equations can be written as below:

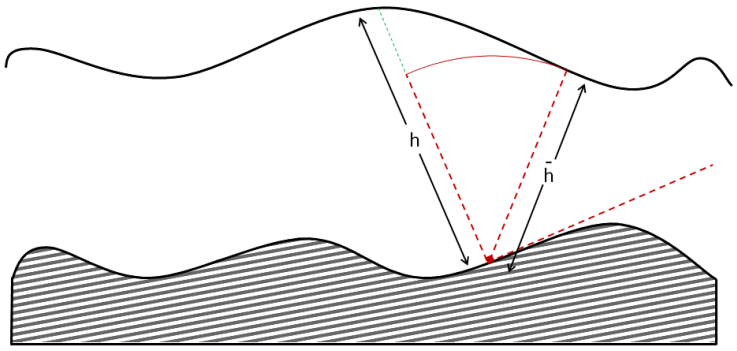


Figure 3.5: Normal distance vs minimum thickness

$$U_S + V_R = 0 \tag{3.62}$$

$$-P_S^* + U_{RR} = 0 \tag{3.63}$$

$$P_R^* = 0 \tag{3.64}$$

$$U|_{R=0} = 0 \qquad V|_{R=0} = 0 \tag{3.65}$$

$$V|_{R=H} = H_T + U|_{R=H} H_S \tag{3.66}$$

$$U_R = 0 \tag{3.67}$$

and

$$-P = \tilde{C}^{-1}\{\frac{K}{\epsilon} - 2HK + H_{SS}\} \tag{3.68}$$

$$P^*(S,T) = -\tilde{C}^{-1}(\frac{K}{\epsilon} - 2HK + H_{SS}) + \frac{A}{H^3} + \frac{B}{H^4} \tag{3.69}$$

The velocity profile and evolution equation are easily derived as before,

$$U = P_S^*(\frac{R^2}{2} - HR), \tag{3.70}$$

where

$$P_S^* = -\tilde{C}^{-1}(\frac{K_S}{\epsilon} - 2H_S K - 2HK_S + H_{SSS}) - \frac{3AH_S}{H^4} - \frac{4BH_S}{H^5},$$

and finally,

$$H_T + \frac{\partial}{\partial S}\{\frac{\tilde{C}^{-1}}{3}(\frac{K_S}{\epsilon} - 2H_S K - 2HK_S + H_{SSS})H^3 + AH_S H^{-1} + \frac{4}{3}BH_S H^{-2}\} = 0\ . \tag{3.71}$$

The two limits are:

Case **I**: $K \sim O(\epsilon)$

$$H_T + \frac{\partial}{\partial S}\{(\frac{\tilde{C}^{-1}}{3}(\tilde{K}_S + H_{SSS})H^3 + AH_S H^{-1} + \frac{4}{3}BH_S H^{-2}\} = 0\ , \tag{3.72}$$

Case **II**: $K \sim O(1)$

$$H_T + \frac{\partial}{\partial S}\{\frac{\tilde{C}^{-1}}{3}K_S H^3 + AH_S H^{-1} + \frac{4}{3}BH_S H^{-2}\} = 0\ . \tag{3.73}$$

The above equations capture thinning/thicking and the rupture processes. For sufficiently thick films (100-1000 Angstroms) van der Waals terms will not play any role. At smaller thickness the film can undergo instability leading to rupture, depending on the size of $A$ & $B$.

# Chapter 4

# THIN FILM WETTING OF AN ELLIPTICAL PARTICLE

In this chapter the evolution equation for the film thickness is integrated in time on an elliptically shaped particle using numerical methods. Previous film evolution studies have been on a flat substrate [4] or a circular particle [12]. In the flat case, the curvature value is zero everywhere, and on a circular particle, the curvature is always constant. The derivative of curvature with respect to arc-length ($k_s$), which is a key parameter in the evolution equation, is zero for both cases. Therefore, it is not possible to see the effect of curvature change on the evolution of the film on the aforementioned shapes.

The primary reason for choosing an ellipse for this analysis is that its curvature is function of the arc-length. This makes $k_s$ non-zero in the evolution equation and allows us to see the effect of variable particle curvature on the gas/liquid interface shape evolution and fluid motion.

In this chapter the evolution equation is integrated in time to calculate both transient and steady state solutions, using MATLAB. The equations are discretized and updated in time using the appropriate MATLAB **ode**-solver.

## *4.1 Liquid Properties*

Molten Aluminum at 954 $K$ has been chosen for the viscous liquid film on top of an elliptical solid that is not deformable. The surface tension is assumed to be constant and gravity has been neglected. The initial film thickness is thick enough that rupture processes should not. The properties of Aluminum have been picked from Anson, Drew and Gruzleski (1999) [17],

Table 4.1: Dimensional parameters for pure aluminum

| Symbol | Description | Al | Units |
|---|---|---|---|
| $T$ | temperature | 954 | K |
| $\rho_L$ | density of liquid | $2.39 \times 10^3$ | Kg m$^{-3}$ |
| $\mu$ | viscosity | $1.2 \times 10^{-3}$ | N s m$^{-2}$ |
| $\nu$ | kinematic viscosity | $5.02 \times 10^{-7}$ | m$^2 s^{-1}$ |
| $\sigma$ | surface tension | 1.007 | N m$^{-1}$ |

Hur, Park and Hirushi (1989) [18] and Dinsdale and Quested (1999) [19] and are tabulated in table 4.1. Representative of other variable are shown in table 4.2. Since the curvature is scaled by its own maximum value, it will be always in the interval of $[0, 1]$, which does not violate the ordering of the perturbation expansion presented in section 3.7. This is another reason that the minimum radius of curvature is the best choice for the length scale in this system compared to other options like the total arc-length or the ellipse diameters.

Table 4.2: Dimensionless parameters and Scales

| Symbol | Description | Definition | Units |
|---|---|---|---|
| $L$ | Length scale | $1/k_{max}$ | m |
| $\epsilon$ | thin film scaling parameter | $h_0/L$ | - |
| $h_0$ | mean film thickness | $\epsilon L$ | m |
| $U_0$ | characteristic tangential velocity | $\mu/(\rho_L h_0)$ | m $s^{-1}$ |
| $V_0$ | characteristic normal velocity | $\epsilon U_0$ | m $s^{-1}$ |
| $T_0$ | Time scale | $L_0/U_0$ | s |
| $Re$ | Reynolds Number | $U_0 h_0/\nu$ | - |
| $\tilde{C}^{-1}$ | Inverse capillary Number | $\epsilon^3 \times \sigma/(\mu U_0)$ | - |

### *4.2 Geometry and Curvature*

The goal of this section is to describe the process of numerically discretizing the elliptical geometry of the ellipse in equal intervals of arc-length. The parametric form of an ellipse is:

$$x = a\cos t \qquad\qquad y = b\sin t \tag{4.1}$$

where $t$ is the polar angle and $a$ and $b$ are the radius of corresponding surrounding and surrounded circles respectively.

In order to have an arc-length domain that is equally divided, the total arc-length has to be calculated first. The arc-length calculation for an ellipse includes an elliptical integral that has to be solved numerically.

$$ds^2 = dx^2 + dy^2 \tag{4.2}$$

$$dx = -a\sin t dt \qquad\qquad dy = b\cos t dt \tag{4.3}$$

$$\frac{ds}{dt} = (a^2 \sin^2 t + b^2 \cos^2 t)^{0.5}$$

$$s_{_T} = \int_0^{2\pi} (a^2 \sin^2 t + b^2 \cos^2 t)^{0.5} dt \tag{4.4}$$

The total arc-length ($s_T$) has to be divided by the number of intervals ($n$) resulting in $n+1$ nodes on the ellipse with an equal amount of an arc-length between them. The value of the polar angle ($t'$) at each node is also required since the curvature can be evaluated analytically as a function of eccentric anomaly (polar angle), although it is not possible to write the curvature analytically as a function of arc-length. Interpolation can be used to determine the corresponding angle at each node. This allows us to evaluate the curvature and its derivative at each node. Interpolation error and the fact that the evolution equation is strongly nonlinear and stiff, can be rendered unimportant by sufficient grid resolution and the choice of numerical scheme. The difference between the angle and the equal arc-length discretization is seen in figure 4.1. An ellipse with $a = 1$ and $b = 0.5$ has been divided into 9 intervals (10 nodes).

The curvature and its derivative with respect to arc-length can be simply calculated by using the following identities.

$$x = a\cos t \qquad\qquad y = b\sin t$$

$$k = \frac{-x''}{y'} \qquad\qquad ds^2 = dx^2 + dy^2$$

where $'$ and $''$ represent the first and second derivative with respect to arc-length, respectively.

$$dx = -a\sin t dt \qquad\qquad dy = b\cos t dt \qquad\qquad \frac{ds}{dt} = \sqrt{a^2 \sin^2 t + b^2 \cos^2 t}$$

By using the chain rule, the curvature of the ellipse is:

$$k = -\frac{ab}{(a^2 \sin^2 t + b^2 \cos^2 t)^{3/2}} \tag{4.5}$$

The minus sign is just because of the notation that has been used in this thesis. Finally, the important parameter in the evolution equation is the derivative of curvature with respect

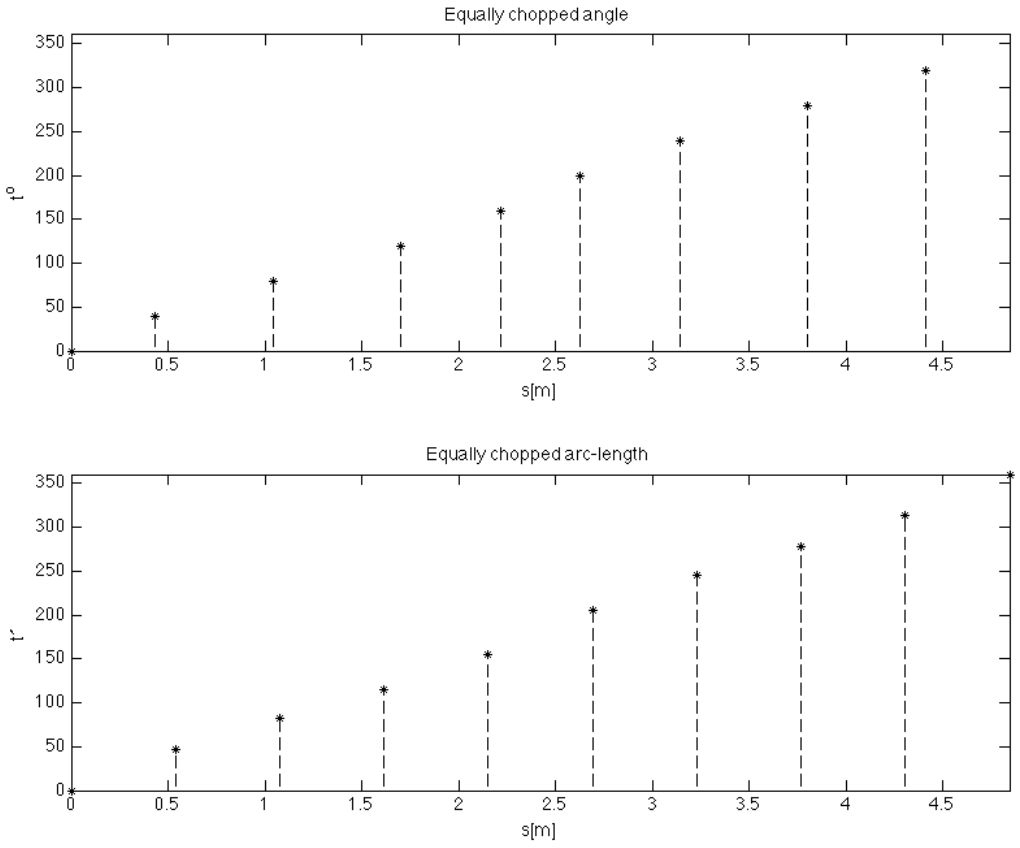


Figure 4.1: domain configuration

to arc-length, which can be derived, using the chain rule again.

$$k_s = -\frac{-3ab(a^2 - b^2)\sin t \cos t}{(a^2 \sin^2 t + b^2 \cos^2 t)^3} \tag{4.6}$$

### *4.3 Discretization method*

In order to simulate the evolution of thickness in time, the evolution equation has to be discretized and numerically integrated in time. A backward finite difference scheme has been used to discretize both curvature and third derivative terms in the evolution equation. All terms in the equation are highly nonlinear due to the existence of the $H^3$ term and

this makes discretization challenging for a forth order PDE. In order to apply the finite difference method the equation 3.57 is rewritten in the form,

$$H_T = (f(H, \tilde{K}_S) + g(H)H_{SSS})_S \tag{4.7}$$

Where:

$$f(H, K_S) = -\frac{1}{3}\tilde{C}^{-1}H^3\tilde{K}_S$$

$$g(H) = -\frac{1}{3}\tilde{C}^{-1}H^3$$

$$\tilde{K}_S = \frac{K_S}{\epsilon}$$

The finite difference approximation used is

$$\begin{aligned}
&(\frac{dH}{dT})_j^n = \\
&(f_{j+1/2} - f_{j-1/2})\frac{1}{(\Delta S)} + \\
&\{g_{j+1/2}(H_{j+2} - 3H_{j+1} + 3H_j - H_{j-1}) - g_{j-1/2}(H_{j+1} - 3H_j + 3H_{j-1} - H_{j-2})\}\frac{1}{(\Delta S)^4}
\end{aligned}$$

Where:

$$f_{j\pm1/2} = \frac{1}{2}(f_j + f_{j\pm1}) \qquad g_{j\pm1/2} = \frac{1}{2}(g_j + g_{j\pm1})$$

As it is shown in the above equations, the numerical scheme will automatically treat the cases **I** and **II**, in which the curvature is of different order in $\epsilon$. In other words, when the curvature $\sim O(1)$, it becomes the dominant term and the third derivative term is automatically neglected and when the curvature is $\sim O(\epsilon)$ both terms are equally important. The spatially discretized evolution equation is the integrated using MATLAB ode-solver (**ode15s**). This ode-solver handles well such nonlinear stiff equations.

### *4.4 Case studies*

In this section, six different particle shapes are introduced, and evolution equations are integrated to give the interface shape over time. One difference between these six ellipses is the major/minor aspect ration. The simulation first treat a circle, in which the curvature is constant everywhere and making the $K_S$ term is zero. The initial film thickness is a cosine superimposing on a circular film. Since it is already known that the steady state solution for the circular substrate is a circle, we can use this case to validate the numerical method that has been presented in the previous section. Subsequently the film evolution is evaluated on five different ellipses characterized by $a$ and $b$. Due to the pressure profile, curvature order changes the thinning mechanism of the system.

$$P(S,T) = -\tilde{C}^{-1}(\frac{K}{\epsilon} + H_{SS}) \tag{4.8}$$

These six different cases have been classified in table 4.3 and they all can be seen together in figure 4.2. Due to the fact that the chosen length scale for the problem is the minimum radius of curvature of the ellipse, many parameters vary from case to case. The nature of these required parameters have been fully explained in table 4.2. For the case of $\epsilon = 0.01$, the values of these parameters have been calculated for each case depending on the curvature and are presented in table 4.4. The absolute values of the dimensionless curvature has been shown for each case separately in figure 4.3. By looking at the curvature profile one can easily understand that the curvature can be of unit order or of $O(\epsilon)$, and also both situations can be found on one ellipse in different places.

Table 4.3: Different cases of study

| Case number | a [m] | b [m] | Dimensionless initial condition |
|---|---|---|---|
| 1 | 1 | 1 | 1+Acos($\omega S$) |
| 2 | 1 | 0.9 | 1 |
| 3 | 1 | 0.7 | 1 |
| 4 | 1 | 0.5 | 1 |
| 5 | 1 | 0.3 | 1 |
| 6 | 1 | 0.1 | 1 |

Table 4.4: The values of scales

| Case Number | L [$m$] | $h_0$[m] | $U_0$[m $s^{-1}$] | Re | $\tilde{C}^{-1}$ |
|---|---|---|---|---|---|
| 1 | 1 | 0.01 | 5.0209E-5 | 1 | 16.7134 |
| 2 | 0.81 | 0.0081 | 6.1987E-5 | 1 | 13.5379 |
| 3 | 0.49 | 0.0049 | 1.0274E-4 | 1 | 8.1896 |
| 4 | 0.25 | 0.0025 | 2.0084E-4 | 1 | 4.1784 |
| 5 | 0.09 | 0.0009 | 5.5788E-4 | 1 | 1.5042 |
| 6 | 0.01 | 0.0001 | 0.005 | 1 | 0.1671 |

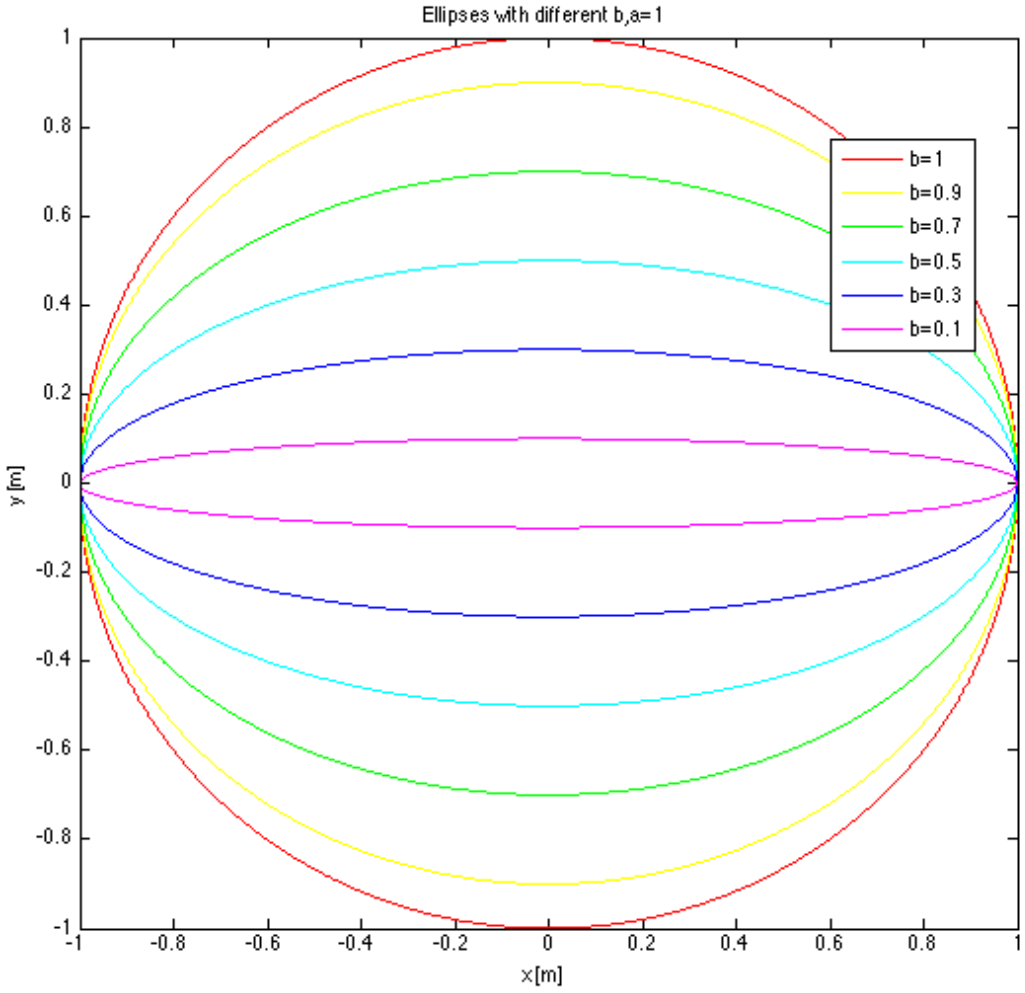


Figure 4.2: Substate shape

For the elliptical cases a uniform film has been chosen as the initial condition. Note that the initial shape of free surface is *not* an ellipse, although it appears very similar. To construct the actual film configuration the normal vector of the solid/liquid interface is needed at each node. The top interface location ($\vec{r_i}$) during time can be expressed by the following equation:

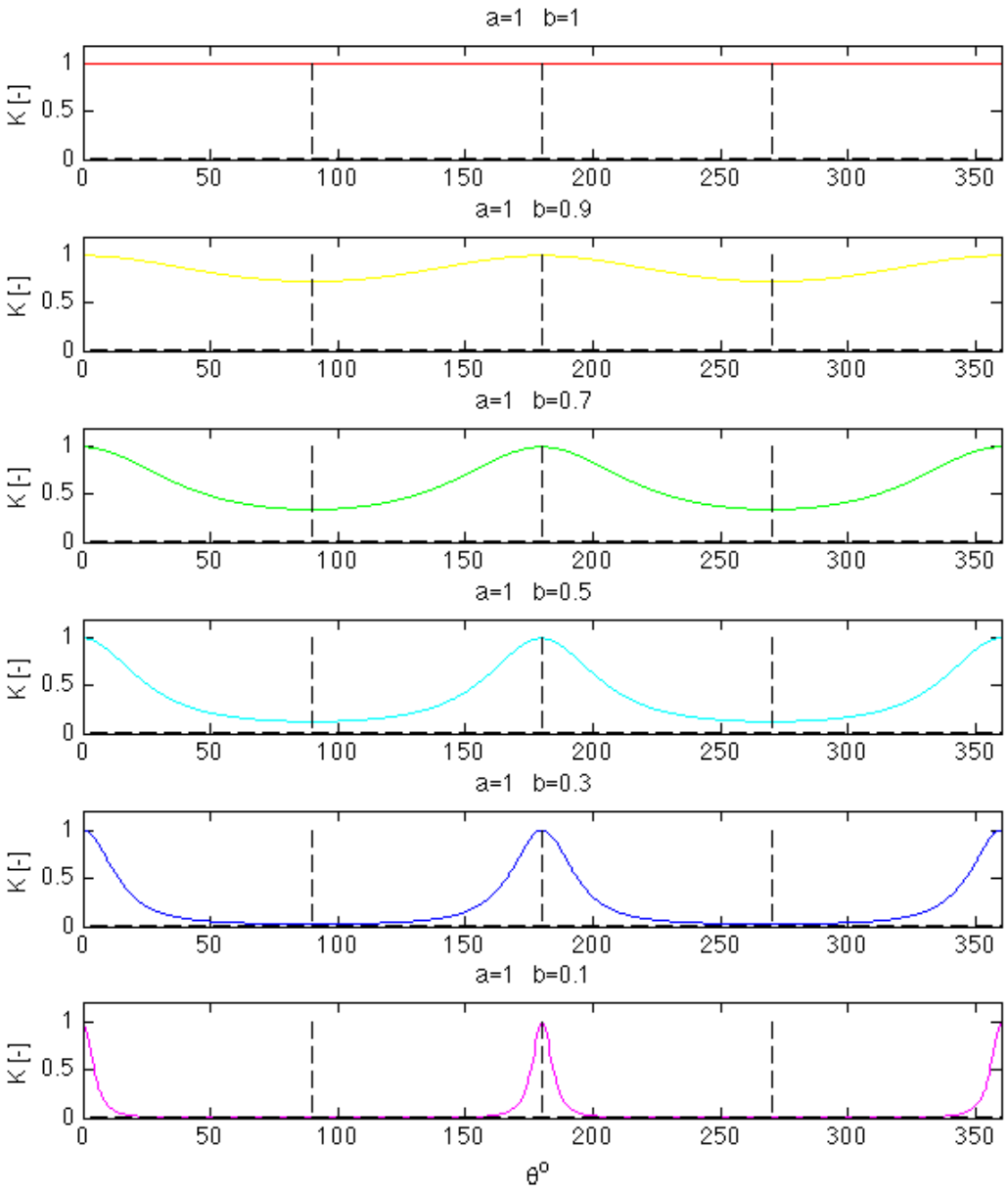


Figure 4.3: Dimensionless curvature

$$\vec{r}_i(s,t) = \vec{r}_p + h(s,t)\hat{n} \tag{4.9}$$

where $\vec{r}_p$ is the solid/liquid interface location

$$\vec{r}_p = a\cos\theta\hat{i} + b\sin\theta\hat{j} \tag{4.10}$$

and $\hat{n}$ is its normal vector,

$$\hat{n} = \frac{1}{N}\{b\cos\theta\hat{i} + a\sin\theta\hat{j}\} \tag{4.11}$$

where

$$N = (a^2\sin^2\theta + b^2\cos^2\theta)^{0.5} \tag{4.12}$$

Here $\theta$ is the eccentric anomaly angle. Using the above equations the top interface location can be expressed in Cartesian coordinates as:

$$x_i = a\cos\theta + \frac{1}{N}bh\cos\theta \qquad y_i = b\sin\theta + \frac{1}{N}ah\sin\theta$$

It can be easily understood from the Cartesian form of the gas/liquid interface that the free surface is not an ellipse. The difference between the uniform film configuration and an ellipse is shown in figure 4.4. In this figure an ellipse with diameters of $a+h$ and $b+h$ has been compared with a uniform film on top of an ellipse with diameters of $a$ and $b$.

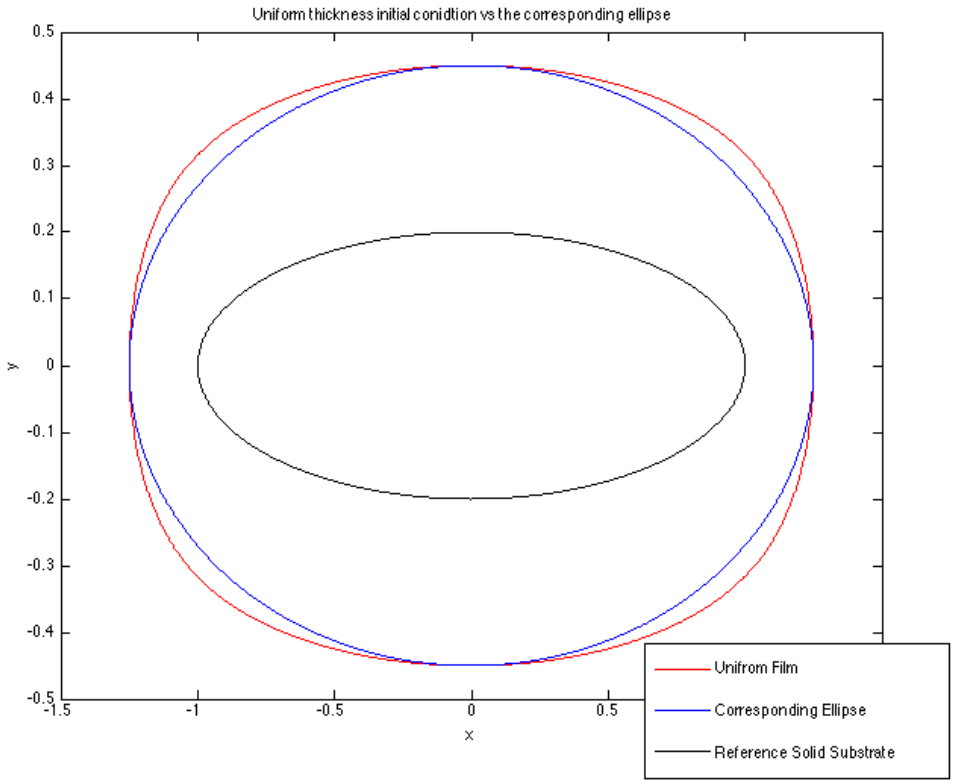


Figure 4.4: Initial condition configuration

## *4.5 Results*

### *4.5.1 Case 1: Circular substrate*

The main goal of simulating the evolution equation on a circular substrate is to use it as a tool to validate the evolution equation, since it is already known that the final steady state solution for this case is the uniform film with constant thickness (another circle around the substrate). To examine the evolution equation, it is needed to start the simulation with a non-uniform initial condition. The initial condition that has been chosen here is a cosine wave generated around mean thickness. The dimensionless form of initial condition can be written as below,

$$H_{initial} = 1 + A\cos(\omega S) \qquad \omega = 5 \qquad A = 0.005$$

As it is shown in figure 4.5, the amplitude becomes smaller over time until it vanishes leaving, a uniform film with constant thickness as was predicted. This results means that the derived evolution equation relaxes to the appropriate final state.

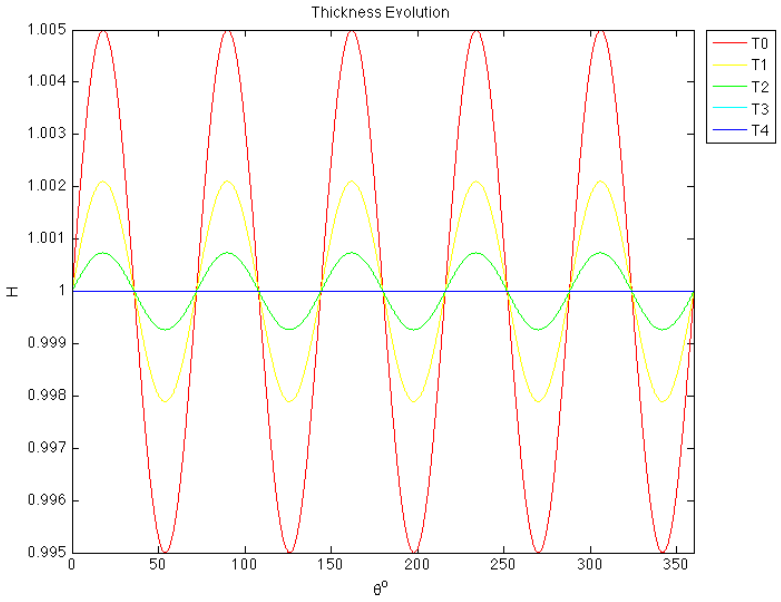


Figure 4.5: Thinning process on circular substrate

### *4.5.2 Case 2: b=0.9*

Cases 2 through 6 are five different ellipses with the same semi-major axis ($a = 1$) and different semi-minor axes ($b$). In the second case $b$ has been chosen to be 0.9, which is closest to the circular case. Decreasing $b$ changes the ellipse shape from a circle to an

increasingly flat ellipse. A thin film with uniform thickness has been chosen as the initial condition for all the elliptical cases. The evolution of thickness for $b = 0.9$ is shown in figure 4.6.

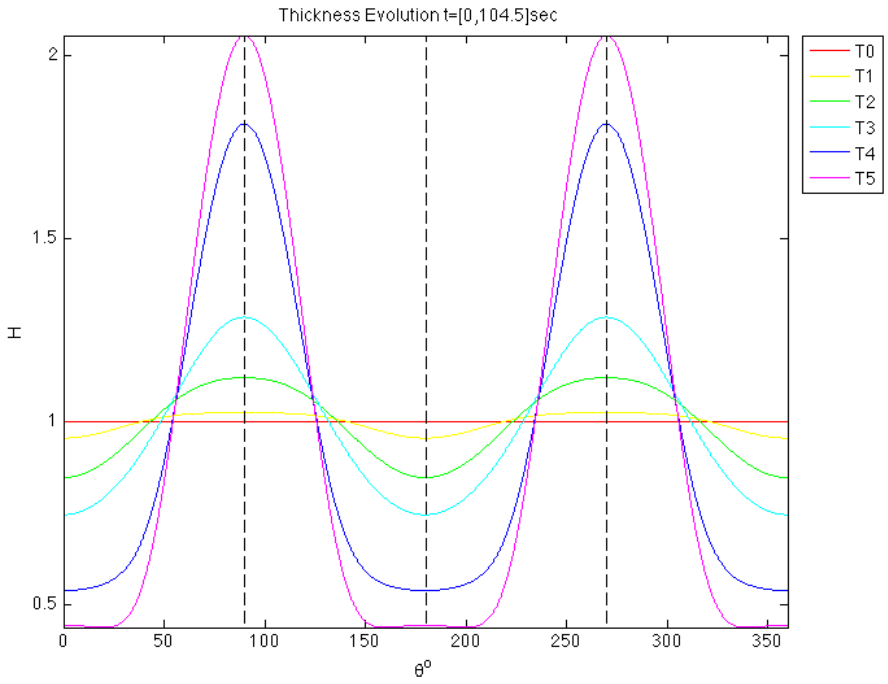


Figure 4.6: Thinning process on an ellipse with a=1 and b=0.9

As can be seen, the film gets thinner near the location $\theta = 0^o$ and thicker near $\theta = 90^o$, which makes sense since the pressure is higher where the curvature is higher and that causes a flow from higher pressure regions to lower pressure ones. This flow changes the interface shape over time, which is shown in figure 4.7. The film thickness has been scaled 10 times larger than the actual size in order to make changes more visible in this plot.

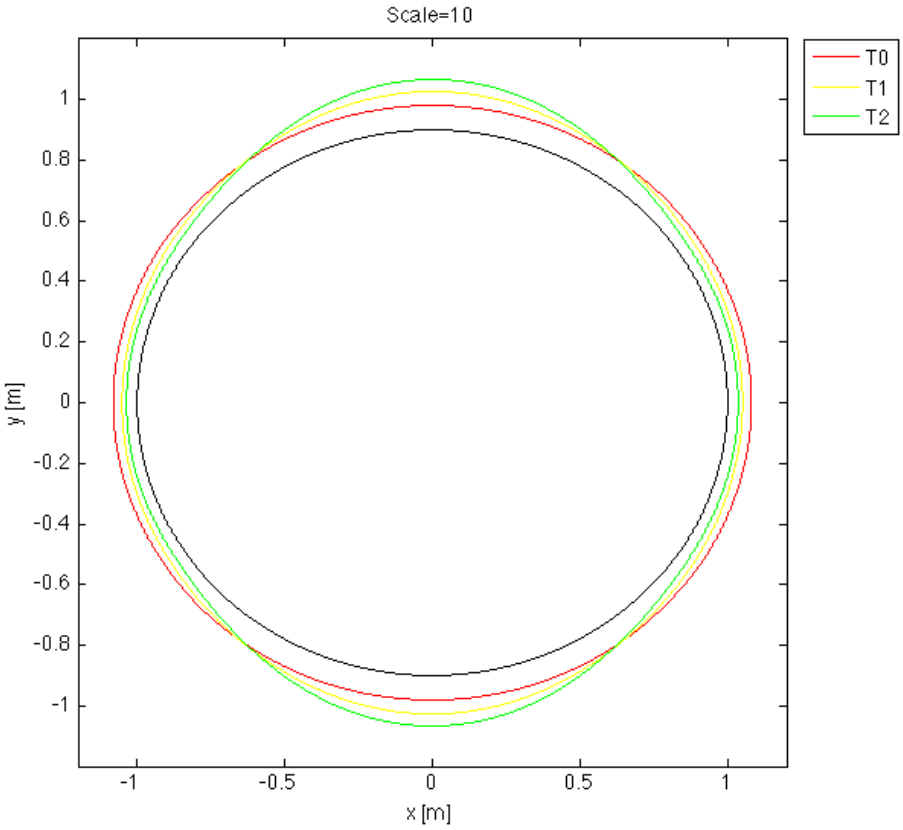


Figure 4.7: Interface Shape

The shapes have not relaxed to equilibrium because by an approximate calculation, it can be shown that the thinning process continues forever. The thinning rate for the symmetric node corresponding to $S = 0$ can be estimated analytically.

Since

$$3H_T + \{\tilde{C}^{-1}(\bar{K}_S + H_{SSS})H^3\}_S = 0 \tag{4.13}$$

$$3H_T = -\tilde{C}^{-1}\{(\bar{K}_{SS} + H_{SSSS})H^3 + 3H_S H^2(\bar{K}_S + H_{SSS})\} \tag{4.14}$$

Then due to the symmetry of the system $H_S$ is always zero at $S = 0$, therefore, the equation

4.14 simplifies to

$$H_T = -\frac{\tilde{C}^{-1}}{3}(\bar{K}_{SS} + H_{SSSS})H^3 \tag{4.15}$$

Approximating

$$\bar{K}_{SS} + H_{SSSS} = \beta \tag{4.16}$$

as a positive constant, then

$$\frac{dH}{dT} = -\alpha H^3 \qquad \alpha = \beta\frac{\tilde{C}^{-1}}{3} \tag{4.17}$$

Finally, the approximate thickness of the film at the first node can be derived by integrating the above equation, giving

$$H^2 = \frac{1}{3\alpha T + 1} \tag{4.18}$$

revealing that $H$ never reaches 0. This equation is validated with numerical results of each case in figure 4.21. Due to the high computational cost of solving the evolution equation, it is impossible to run the code for very long timespans. However, the equation 4.18 reveals that the thinning process will never stop.

Equation 4.18 also indicate that van der Waals forces are mandatory for rupture to occur and the thinning process ensures that the film will eventually become thin enough so that van der Waals forces become important. The thinning rate is highly dependent on the geometry of the ellipse and surface tension, which play their roles through capillary number, the curvature and the interface shape. The required time to reach the thickness for which that van der Waals forces come into play, depends on $\alpha$ and on the initial thickness.

Since it is not possible to integrate the thickness for an infinite amount of time, the simulation has been continued, up to the point that the thinning rate becomes small enough that equation 4.18 is obeyed. Whether the simulation has been continued for enough time or not, can be checked by plotting the $Ln(H)$ vs $Ln(T)$ of the first node over time, which is shown in figure 4.21 in the end of this chapter. In figure 4.8 the thickness settles into $T^{-1/2}$ behavior after an initial transient, this is more clear for all case studies in figure 4.21.

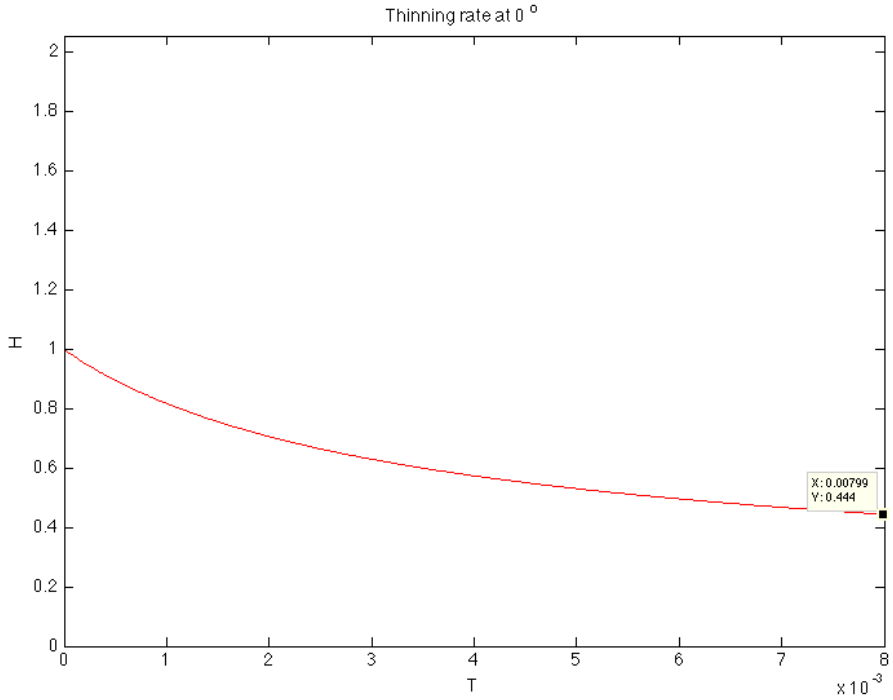


Figure 4.8: Thinning process at $0^o$ $T_0 = 1.3067E + 4[sec]$

### *4.5.3 Case 3: b=0.7*

Evolution of the thickness of the film over time for this case is shown in figure 4.9. While the thinning is happening at $0^o$, which has high curvature, the film gets thicker around $90^o$. The main difference between this case and previous one is that during the process, the maximum is not exactly at $90^o$, however, the two local maxima are getting closer to each other over time until they meet exactly at $90^o$. This creates a surface wave on the top interface, which starts around high curvature regions and ends around $90^o$. This process is shown more clearly in figure 4.10.

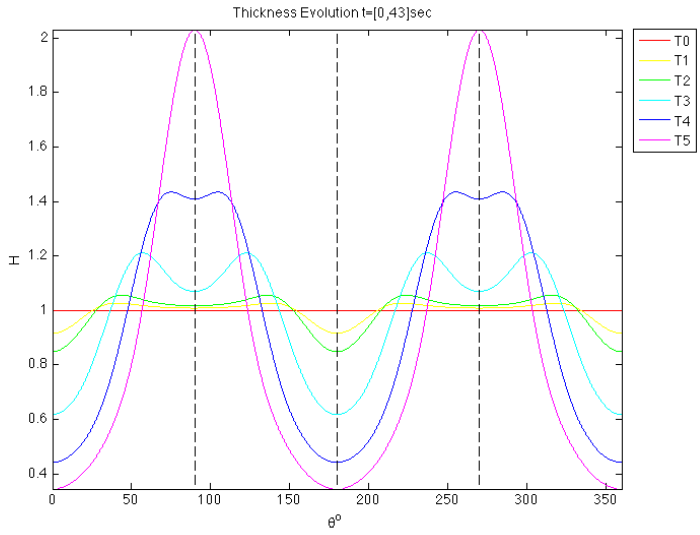


Figure 4.9: Thinning process on an ellipse with a=1 and b=0.7

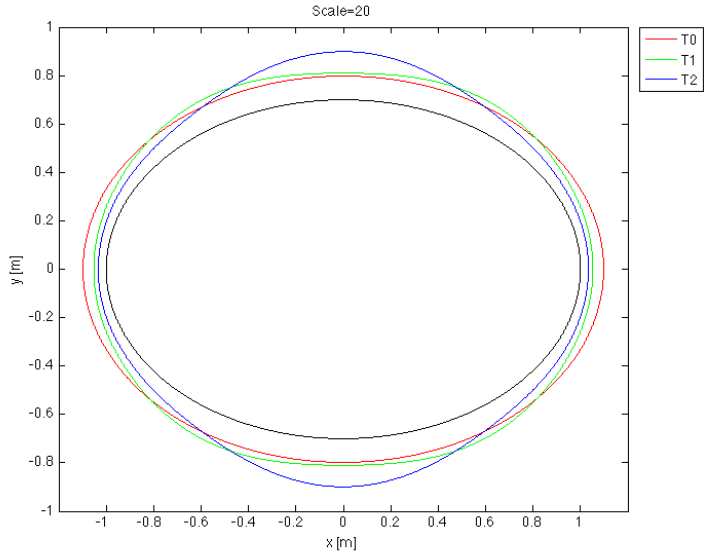


Figure 4.10: Interface Shape

It worth mentioning that as the aspect ratio of the ellipse increases the thinning process happens faster, in other words the system evolves more rapidly. For instance, this process

takes around 100 seconds for the case of $b = 0.9$ and around 40 seconds for this case. The velocity scale values listed in table 4.4 is an indicator of this behavior. Note that although the thinning process gets very slow after a certain amount of time, there might be still some process going on in low curvature regions. The thinning process of the first node is shown in figure 4.11.

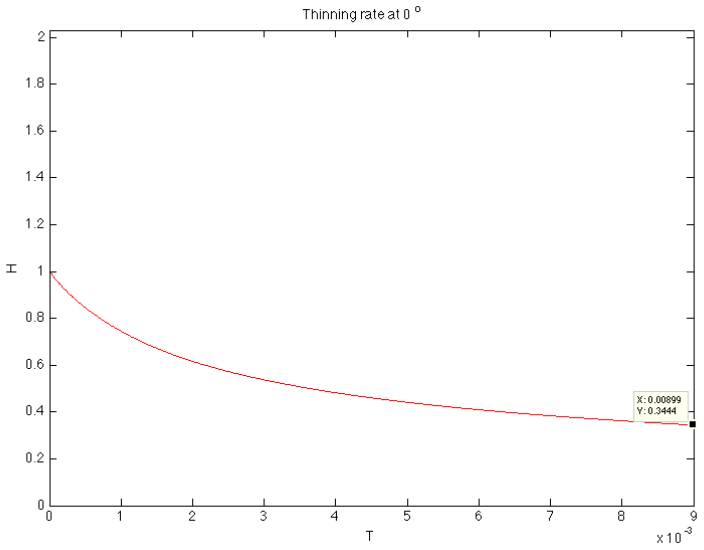


Figure 4.11: Thinning process at $0^o$ $T_0 = 4.7820E + 3[sec]$

### *4.5.4 Case 4: b=0.5*

The interface evolution over time for this case is shown in figure 4.12. Although the thinning process around the high curvature regions is similar to the previous cases (but faster), the maximum is not located at $90^o$ even at the final simulated time step. The big question here is that if it was possible to run the code for a very long time the maximum location

would move to $90^o$ or not, in other words would the two visible bumps in figure 4.13 would meet each other or possibly continue to move around the film perimeter. This question can be also asked about the other two following cases, in which the aspect ratio increases even more. Another interesting observation about this case is that a local maximum gets created around at $90^o$ in the fifth plot ($T_4$) but disappears after some time. It can be questioned that this is just a numerical issue or it has also some physical meanings.

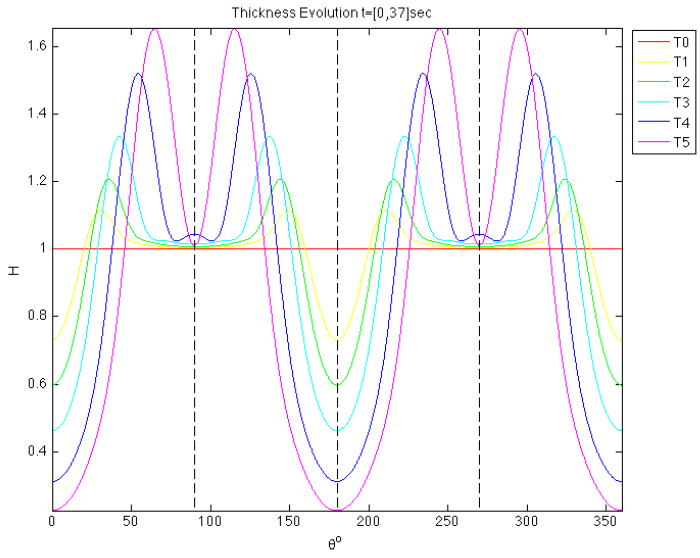


Figure 4.12: Thinning process on an ellipse with a=1 and b=0.5

### *4.5.5 Case 5: b=0.3*

Film thickness is shown over time for this case in figure 4.15. The questions that have been discussed in the previous case can also be asked about this case. The code for this case was running for a very long time ( 24 hours). That is the reason of the fact that the final thickness is evaluated at 322 seconds and it does not mean that the thinning process in this case is slower than in previous cases since it happens in the earlier time steps and after a while it does not change that much. The surface waves exist also in this case and they are shown in figure 4.16 50 times bigger than their actual size. Another interesting point that

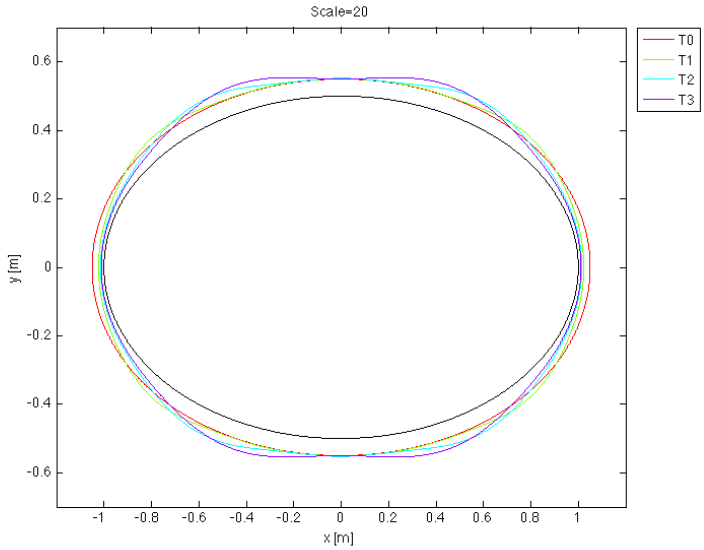


Figure 4.13: Interface Shape

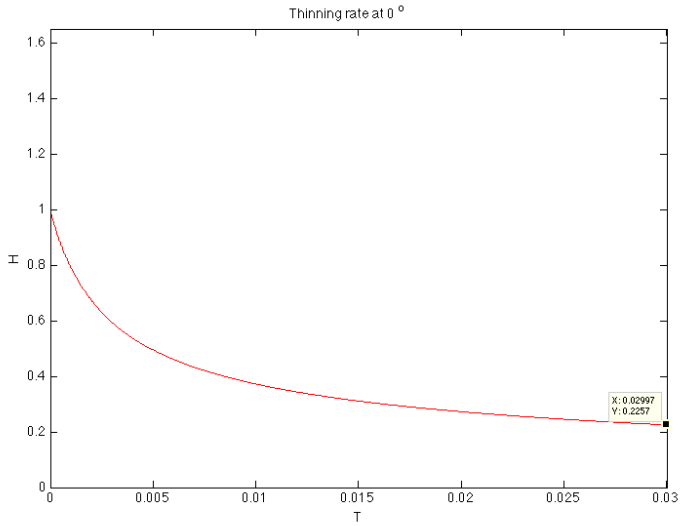


Figure 4.14: Thinning process at $0^o$ $\quad T_0 = 1.2448E + 3[sec]$

has to be investigated for case 5 is that for the final simulation the thickness becomes less than the initial condition at $90^o$, which is unexpected. The thinning process around high

curvature regions is similar to previous cases and will get very slow after some time. As it is shown in figure 4.17, the thickness at $0^o$ gets close to 0.04 of its initial value, which might be thin enough to make rupture happen depending on the initial thickness.

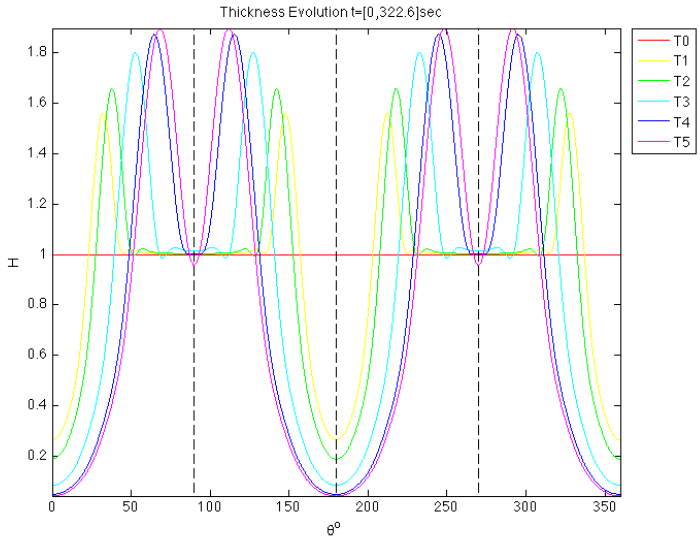


Figure 4.15: Thinning process on an ellipse with a=1 and b=0.3

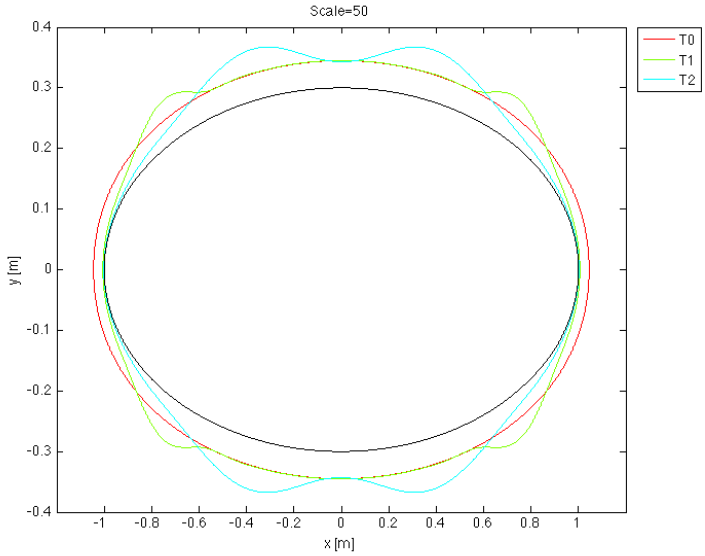


Figure 4.16: Interface Shape

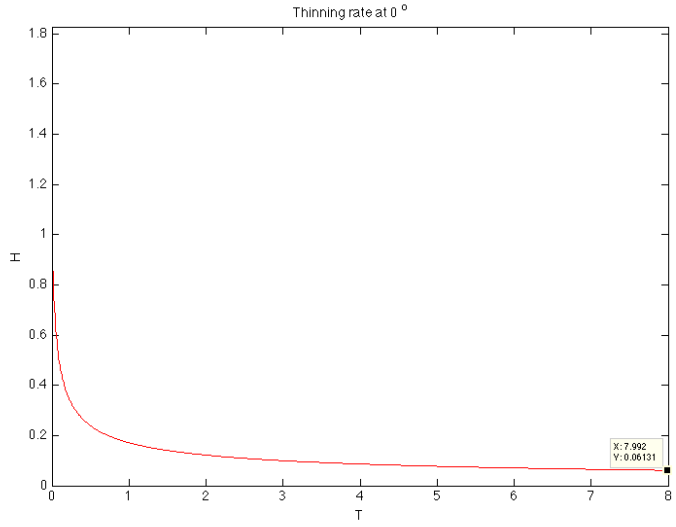


Figure 4.17: Thinning process at $0^o$ $\quad T_0 = 161.32[sec]$

### *4.5.6 Case 6: b=0.1*

The aspect ratio is very high in this calculation so that the low curvature regions can be assumed almost flat. This explains why the thickness does not change in those regions as shown in figure 4.18. In addition the volume of fluid near the high curvature regions is very small compared to the fluid volume at the low curvature regions. Thus, although there is a rapid thinning near $0^o$ there is much slower dynamic's $90^o$.

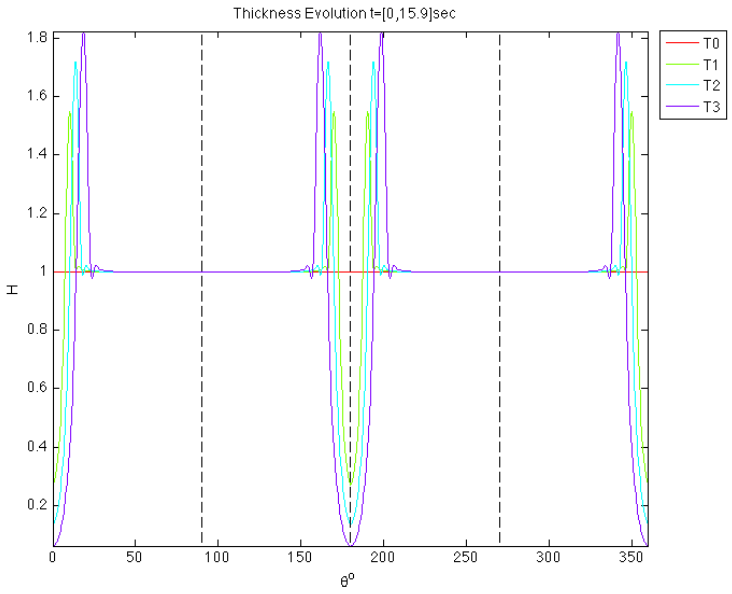


Figure 4.18: Thinning process on an ellipse with a=1 and b=0.1

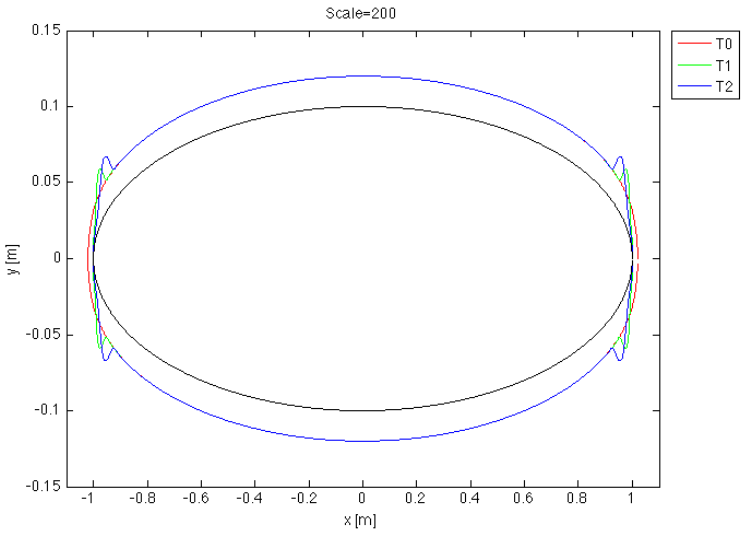


Figure 4.19: Interface Shape

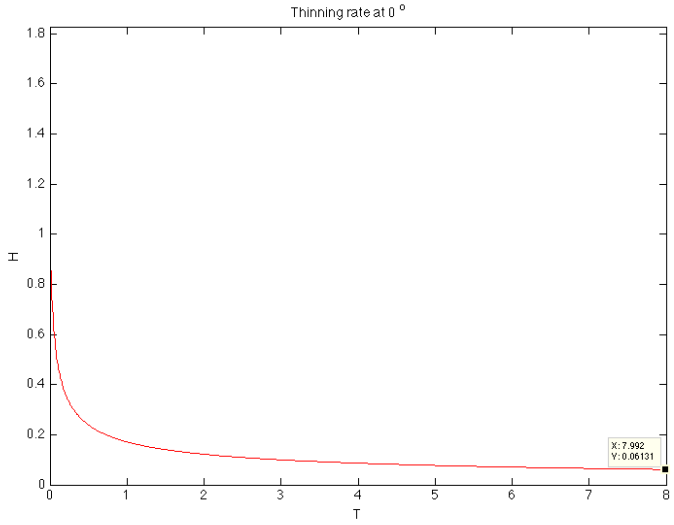


Figure 4.20: Thinning process at $0^o$ $\quad T_0 = 1.9917[sec]$

Finally, the pressure (3.55) helps to identify a common pattern of the results for all five different ellipses. In all cases the interface shape changes over time in such a way that $H_{SS}$

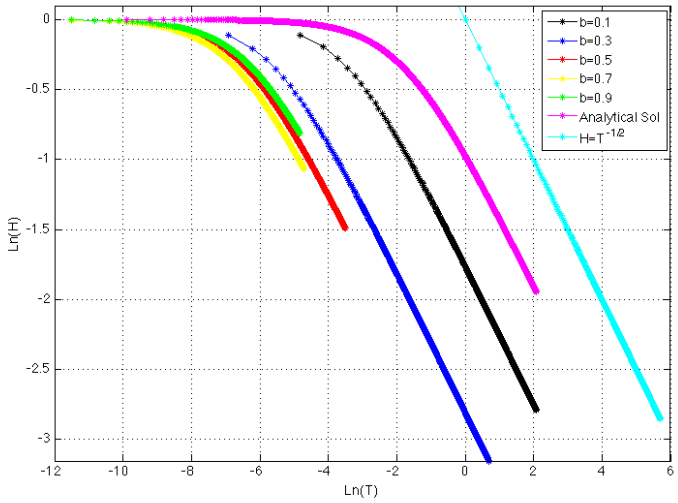


Figure 4.21: Numerical solution of symmetric node vs Analytical Solution

increases at $0^o$ and $180^o$, thereby decreasing the pressure in these high-pressure regions. The value of $H_{SS}$ also decreases from its initial value by increasing film thickness near the intersection of the semi-minor axis and the ellipse surface, thereby increasing the pressure in these low-pressure areas. The dynamic's of the film acts to change the pressure toward a more balance situation. However, the pressure never becomes exactly uniform everywhere and the thinning process continues forever, or until rupture.

# Chapter 5

# SUMMARY, CONCLUSIONS AND FUTURE WORK

## *5.1 Summary and Conclusion*

Thin wetting liquid films on solid particles including effects such as viscous forces and surface tension are investigated in this thesis. Simpler free surface problems are described such as a thin film on a flat substrate in order to produce the required understanding to start working on more complicated problems, such as thin films on solid substrate of any given shape. The role of surface tension, viscous forces and intermolecular forces, are studied included the in free surface boundary conditions and fluid mechanics governing equations for the flat substrate. Lubrication theory and dimensional analysis are used to simplify the equations in order to find the the pressure profile, the axial component of velocity and finally the evolution equation for the film thickness over time. The dimensionless forms of these equations for the simple flat substrate case with neither gravity nor van der Waals forces included, in Cartesian coordinates are:

$$P(X,T) = -\tilde{C}^{-1} H_{XX}$$

$$U = P_X(\frac{Z^2}{2} - HZ)$$

$$3H_T + \tilde{C}^{-1}(H_{XXX}H^3)_X = 0$$

The surface tension play its role through the capillary number ($\tilde{C}$) ). The literature research has focused on flat and circular substrates. The substrate curvature is constant for both aforementioned cases. This research explores the general case of a particle having variable curvature and it is seen that the variation in the curvature of the particle surface acts as a forcing term driving fluid motion. Due to the geometry Cartesian coordinates

are not very useful in dealing with thin films on solid substrates having arbitrary shape. This research adopts a normal-tangential coordinate system, in which arc-length measured on the solid/liquid interface and normal distance from it, are the independent variables. Conservation of mass, the Stokes flow equations and all interface conditions are derived in the new coordinate system. Derived equations are simplified using dimensional analysis and lubrication theory providing leading order set of governing equations and boundary conditions. The ratio of mean thickness to minimum radius of curvature of the solid substrate ( $\epsilon$) is chosen as the proper expansion parameter for the dependent variables.The pressure profile, the tangential component of velocity and evolution equation are derived for solid substrates with any shapes excluding those which have sharp corners. The dimensionless forms of these equations are:

$$P(S,T) = -\tilde{C}^{-1}(\frac{K}{\epsilon} + H_{SS})$$

$$U(S,T) = P_S(\frac{R^2}{2} - HR)$$

$$3H_T + \frac{\partial}{\partial S}\{(\tilde{C}^{-1}(\tilde{K}_S + H_{SSS})H^3\} = 0$$

where $K$ is the dimensionless form of particle curvature. The pressure equation is validated analytically by comparison of the circular case [12]. The evolution equation is also derived including van der Waals forces, which can allow for rupture processes,

$$H_T + \frac{\partial}{\partial S}\{(\frac{\tilde{C}^{-1}}{3}(\tilde{K}_S + H_{SSS})H^3 + AH_SH^{-1} + \frac{4}{3}BH_SH^{-2}\} = 0$$

The results here do study the effects of intermolecular forces. Numerical methods are used to simulate the evolution of thickness of a wetting thin film over time on elliptically shaped particles. Due to the variable curvature, which changes along the ellipse arc-length, there are high-pressure and low-pressure regions. This pressure gradient causes a flow, which

changes the gas/liquid interface shape. The gas/liquid interface is plotted over time for ellipses with different aspect ratios. The code has also been applied to a circular particle with a non-constant initial condition for validation.

The derived pressure equation indicates that pressure is higher where the absolute value of curvature is higher and lower around low curvature regions. For an elliptically shaped substrate, starting with a uniform film thickness, the $H_{SS}$ term is zero in the beginning; therefore, the pressure is higher around high curvature regions which are located at the intersection of semi-major axis and the ellipse. The flow caused by the pressure gradient changes the interface shape in a way that $H_{SS}$ increases in time. As $H_{SS}$ term increases the pressure value decreases in high curvature regions and increases in low curvature region as the system tries to balance pressure. All the results for ellipses follow this pattern. The value of $H_{SS}$ also decreases from its initial value by increasing thickness around the intersection of semi-minor axis and the ellipse. As the aspect ratio of the ellipse ($a/b$) increases, the maximum thickness tends to locate further from the maximum curvature point at the final simulated time step.

As shown in the result section the thickness at $0^o$ becomes thinner over time. This thinning process becomes very slow after some time but never stops, which can be seen in all of the plots that show the thinning process over time at $0^o$. The approximate analytical analysis that has been done in the result section also validates the fact that the thinning process will continue forever and the thickness will not reach to zero in finite time, therefore, the system will never get to a steady state. The fact that the thickness in thinning regions continues means at some point that van der Waals or other intermolecular forces will become important that may cause rupture in a finite amount of time or that will give rise to a disjoining pressure that will render the effective pressure $P^*$ constant everywhere, so that the liquid film has reached equilibrium.

## *5.2 Future Work*

The very first thing that needs to be done is writing a program to monitor the pressure profile over time. This would allow us to understanding about the flow direction and its effect on the interface shape.

In order to run the code for longer time it is necessary to write a more efficient program. Since we are dealing with periodic boundary conditions spectral methods could be more convenient compare to finite difference methods. Fast Fourier transforms are usually very helpful in dealing with stiff partial differential equations; however the non-linearity could still be an issue. By having a faster program that uses less amount of memory would make it possible to answer the discussed questions related to the surface waves that occur on the top interface as the aspect ratio of the ellipse increases.

To simulate the rupture process the program must be modified to include the effect of van der Waals or other short range forces. This would enable us to see an interface shape that is thinning, develop an instability that leads to film rupture.

Since the evolution equation describes the thinning process on solid substrates of any given shape (excluding the ones which have sharp corners), it will be interesting to see the interface shape on different particles other than elliptically shaped ones; could particle shapes be designed to cause specific flow behaviors?

It is also interesting to see what happens if the initial condition is not uniform everywhere in other words, what would be the interface shape before the rupture if the initial condition is not symmetric? An example might be a particle that has been withdrawn from a liquid bath.

Appendix A

# APPENDIX

## *A.1 Curvature of the top interface*

In this section the curvature at the top interface has been calculated from 3 different methods:

- Direct geometrical method ($d\theta_i/ds_i$)
- Dot product of unit normal of the top interface and the derivative of unit tangent vector with respect to arc-length of the top interface ($\hat{n}_i.dt_i/ds_i$).
- Divergence of the unit normal of the top interface ($-\nabla.\hat{n}_i$).

### *A.1.1 Direct geometrical method*

This method calculates the curvature of the interface by taking the derivative of the top interface tangent angle $\theta_i$ with respect to its own arc-length $s_i$. It is easier to find the derivative of $\theta_i$ with respect to the bottom interface arc-length $s$ first, and then derive the curvature using a simple chain rule.

$$k_i = \frac{d\theta_i}{ds_i} = \frac{d\theta_i}{ds}\frac{ds}{ds_i} \tag{A.1}$$

$\theta_i$ is the angle between $\hat{t}_i$ and the horizon, and can be derived as below

$$\hat{t}_i = \frac{1}{N}\{(1-h\theta_s)\hat{t} + h_s\hat{n}\} \quad N^2 = (1-h\theta_s)^2 + h_s^2$$

$$\hat{t} = \cos\theta\hat{i} + \sin\theta\hat{j} \quad \hat{n} = -\sin\theta\hat{i} + \cos\theta\hat{j}$$

$$\hat{t}_i = \frac{1}{N}\{((1-h\theta_s)\cos\theta - h_s\sin\theta)\hat{i} + ((1-h\theta_s)\sin\theta + h_s\cos\theta)\hat{j}\}$$

$$\theta_i = \arctan\{\frac{(1-h\theta_s)\sin\theta + h_s\cos\theta}{(1-h\theta_s)\cos\theta - h_s\sin\theta}\} \tag{A.2}$$

It is straightforward to calculate the first term of A.1 after finding $\theta_i$,

$$\theta_i = \arctan(\frac{f}{g}) \Longrightarrow \frac{d\theta_i}{ds} = \frac{f'g + g'f}{f^2 + g^2}$$

$$f = (1 - h\theta_s)\sin\theta + h_s\cos\theta \qquad g = (1 - h\theta_s)\cos\theta - h_s\sin\theta$$

$$f' = \frac{df}{ds} = -2h_s\theta_s\sin\theta - h\theta_{ss}\sin\theta + \theta_s(1 - h\theta_s)\cos\theta + h_{ss}\cos\theta$$

$$g' = \frac{dg}{ds} = -\{2h_s\theta_s\cos\theta + h\theta_{ss}\cos\theta + \theta_s(1 - h\theta_s)\sin\theta + h_{ss}\sin\theta\}$$

After all possible simplifications the derivative of the top-interface tangent angle with respect to the reference arc-length is:

$$\frac{d\theta_i}{ds} = \frac{1}{N^2}(\theta_s(1 - h\theta_s)^2 + h_{ss}(1 - h\theta_s) + 2h_s^2\theta_s + hh_s\theta_{ss}) \tag{A.3}$$

To find the rate of change of reference arc-length with respect to top interface arc-length $ds/ds_i$, some basic arc-length calculus is needed that is listed below. In order to make the calculation more clear the reference arc-length $s$ has been changed to $s_p$ during this section.

$$\vec{r_i} = (x_p - h\sin\theta)\hat{i} + (y_p + h\cos\theta)\hat{j} \tag{A.4}$$

$$\frac{dx_p}{ds_p} = \cos\theta \tag{A.5}$$

$$\frac{dy_p}{ds_p} = \sin\theta \tag{A.6}$$

$$dx_i = dx_p - dh\sin\theta - hd\theta\cos\theta \qquad dy_i = dy_p + dh\cos\theta - hd\theta\sin\theta$$

$$ds_i^2 = dx_i^2 + dy_i^2 \tag{A.7}$$

$$ds_p^2 = dx_p^2 + dy_p^2 \tag{A.8}$$

$$ds_i^2 = dx_p^2 + (dh)^2\sin^2\theta + (hd\theta)^2\cos^2\theta - 2\sin\theta dx_p dh - 2h\cos\theta d\theta dx_p + 2h\sin\theta\cos\theta dh d\theta + ...$$

$$dy_p^2 + (dh)^2\cos^2\theta + (hd\theta)^2\sin^2\theta + 2\cos\theta dy_p dh - 2h\sin\theta d\theta dy_p - 2h\sin\theta\cos\theta dh d\theta$$

$$ds_i^2 = ds_p^2 + dh^2 + (hd\theta)^2 + 2dh[\cos\theta dy_p - \sin\theta dx_p] - 2hd\theta[\cos\theta dx_p + \sin\theta dy_p]$$

Divide both sides by $ds_p^2$ :

$$(\frac{ds_i}{ds_p})^2 = 1 + (\frac{dh}{ds})^2 + h^2(\frac{d\theta}{ds_p})^2 + 2\frac{dh}{ds}[\cos\theta\frac{dy_p}{ds_p} - \sin\theta\frac{dx_p}{ds_p}] - 2h\frac{d\theta}{ds_p}[\cos\theta\frac{dx_p}{ds_p} + \sin\theta\frac{dy_p}{ds_p}]$$

By using equations , :

$$(\cos\theta\frac{dy_p}{ds_p} - \sin\theta\frac{dx_p}{ds_p}) = 0 \quad , \quad (\cos\theta\frac{dx_p}{ds_p} + \sin\theta\frac{dy_p}{ds_p}) = 1 \tag{A.9}$$

Back to previous notation: $s_p \to s$

$$(\frac{ds_i}{ds})^2 = 1 + (h\theta_s)^2 - 2h\theta_s + h_s^2 = (1 - h\theta_s)^2 + h_s^2$$

$$\frac{ds}{ds_i} = \{(1 - h\theta_s)^2 + h_s^2\}^{-1/2} = N^{-1} \tag{A.10}$$

Finally by using chain rule:

$$k_i = \frac{d\theta_i}{ds_i} = \frac{(\theta_s(1 - h\theta_s)^2 + h_{ss}(1 - h\theta_s) + 2h_s^2\theta_s + hh_s\theta_{ss})}{\{(1 - h\theta_s)^2 + h_s^2\}^{3/2}} \tag{A.11}$$

*A.1.2 Dot product of unit normal and the derivative of unit tangent vector*

$$k_i = \hat{n}_i.\frac{d\hat{t}_i}{ds_i} \tag{A.12}$$

$$\hat{t}_i = \frac{1}{N}\{(1 - h\theta_s)\hat{t} + h_s\hat{n}\} \qquad \hat{n}_i = \frac{1}{N}\{-h_s\hat{t} + (1 - h\theta_s)\hat{n}\} \qquad N = \{h_s^2 + (1 - h\theta_s)^2\}^{1/2}$$

Note that in this method we work with the equations including $h$, so we are only working with the interface curve not the family of curves.

$$\frac{d\hat{t}_i}{ds_i} = \frac{d\hat{t}_i}{ds}.\frac{ds}{ds_i}$$

$$\frac{d\hat{t}_i}{ds} = \frac{d}{ds}\{\frac{1-h\theta_s}{N}\hat{t}\} + \frac{d}{ds}\{\frac{h_s}{N}\hat{n}\} = \frac{d}{ds}\{\frac{1-h\theta_s}{N}\}\hat{t} + \frac{1-h\theta_s}{N}\frac{d\hat{t}}{ds} + \frac{d}{ds}\{\frac{h_s}{N}\}\hat{n} + \frac{h_s}{N}\frac{d\hat{n}}{ds}$$

where:

$$\frac{d\hat{t}}{ds} = \theta_s\hat{n} \qquad \frac{d\hat{n}}{ds} = -\theta_s\hat{t}$$

$$\frac{d\hat{t}_i}{ds} = N^{-2}\{-(h_s\theta_s + h\theta_{ss})N - N_s(1-h\theta_s)\}\hat{t} + \frac{\theta_s(1-h\theta_s)}{N}\hat{n} + N^{-2}\{(h_{ss}N - N_sh_s)\}\hat{n} - \frac{\theta_sh_s}{N}\hat{t}$$

where:

$$N_s = \frac{dN}{ds} = \{h_{ss}h_s - (h_s\theta_s + h\theta_{ss})(1-h\theta_s)\}N^{-1}$$

$$\frac{d\hat{t}_i}{ds} = \{-(h_s\theta_s + h\theta_{ss})N^{-1} - \{h_{ss}h_s - (h_s\theta_s + h\theta_{ss})(1-h\theta_s)\}(1-h\theta_s)N^{-3}\hat{t} - \theta_sh_sN^{-1}\}\hat{t}$$

$$+ \{\theta_s(1-h\theta_s)N^{-1} + h_{ss}N^{-1} - \{h_{ss}h_s - (h_s\theta_s + h\theta_{ss})(1-h\theta_s)\}h_sN^{-3}\}\hat{n} \qquad \text{(A.13)}$$

Now it is possible to get the dot product:

$$\hat{n}_i = \frac{1}{N}\{-h_s\hat{t} + (1-h\theta_s)\hat{n}\}$$

$$\hat{n}_i.\frac{d\hat{t}_i}{ds} = (h_s^2\theta_s + hh_s\theta_{ss})N^{-1} + \{h_{ss}h_s^2 - (h_s^2\theta_s + hh_s\theta_{ss})(1-h\theta_s)\}(1-h\theta_s)N^{-3} + \theta_sh_s^2N^{-1}$$

$$+ \theta_s(1-h\theta_s)^2N^{-1} + h_{ss}(1-h\theta_s)N^{-1} - \{h_{ss}h_s^2 - (h_s^2\theta_s + hh_s\theta_{ss})(1-h\theta_s)\}(1-h\theta_s)N^{-3}$$

After the simplification and using the chain rule:

$$k_i = \hat{n}_i.\frac{d\hat{t}_i}{ds_i} = \hat{n}_i.\frac{1}{N}\frac{d\hat{t}_i}{ds}$$

$$k_i = \hat{n}_i.\frac{d\hat{t}_i}{ds_i} = \frac{(\theta_s(1-h\theta_s)^2 + h_{ss}(1-h\theta_s) + 2h_s^2\theta_s + hh_s\theta_{ss})}{\{(1-h\theta_s)^2 + h_s^2\}^{3/2}} \qquad \text{(A.14)}$$

Which is exactly the answer that has been derived from the direct geometrical method (method 1).

*A.1.3 Divergence of the normal vector*

$$k_i = -\nabla.\hat{n}_i \tag{A.15}$$

where:

$$\hat{n}_i = \frac{1}{N}\{-h_s\hat{t} + (1 - r\theta_s)\hat{n}\} \qquad N = \{h_s^2 + (1 - r\theta_s)^2\}^{1/2}$$

Note that in this section the $N$ is function of $r$ and $s$. Essentially we work with the family of curves, and in the end set $r = h$ to pick the top interface curve among them.

The fluid dynamics by Z.U.A Warsi has been used to calculate the divergence of a vector:

$$DivA = \frac{1}{h_1 h_2}\{\frac{\partial}{\partial s}(h_2 A_1) + \frac{\partial}{\partial r}(h_1 A_2)\}$$

For our coordinate system $h_1$ and $h_2$ are:

$$h_1 = 1 - r\theta_s \qquad h_2 = 1$$

The important thing about this part is that in order to produce the curvature at the top interface the derivative has been taken with respect to $s$ and not $s_i$.

$$\nabla.\hat{n}_i = \frac{1}{1 - r\theta_s}\{-\frac{\partial}{\partial s}(\frac{h_s}{N}) + \frac{\partial}{\partial r}(\frac{(1 - r\theta_s)^2}{N})\} \tag{A.16}$$

$$\nabla.\hat{n}_i = \frac{N^{-2}}{1 - r\theta_s}\{-(h_{ss}N - N_s h_s) - 2\theta_s(1 - r\theta_s)N - N_r(1 - r\theta_s)^2\}$$

where:

$$N_s = \frac{\partial N}{\partial s} = \{h_{ss}h_s - r\theta_{ss}(1 - r\theta_s)\}N^{-1} \qquad N_r = \frac{\partial N}{\partial r} = -\theta_s(1 - r\theta_s)N^{-1}$$

$$\nabla.\hat{n}_i = \frac{1}{1 - r\theta_s}\{-h_{ss}N^{-1} + (h_{ss}h_s^2 - rh_s\theta_{ss}(1 - r\theta_s))N^{-3} - 2\theta_s(1 - r\theta_s)N^{-1} + \theta_s(1 - r\theta_s)^3N^{-3}\}$$

In order to compare the result with previous methods some simplification is needed.

$$\nabla.\hat{n}_i = \frac{N^{-3}}{1 - r\theta_s}\{-h_{ss}N^2 + h_{ss}h_s^2 - rh_s\theta_{ss}(1 - r\theta_s) - 2\theta_s(1 - r\theta_s)N^2 + \theta_s(1 - r\theta_s)^3\}$$

Now we have to plug in the $N^2$ into the equation:

$$\nabla.\hat{n}_i = \frac{N^{-3}}{1 - r\theta_s}\{-h_{ss}h_s^2 - h_{ss}(1 - r\theta_s)^2 + h_{ss}h_s^2 - rh_s\theta_{ss}(1 - r\theta_s)$$

$$- 2\theta_s h_s^2(1 - r\theta_s) - 2\theta_s(1 - r\theta_s)^3 + \theta_s(1 - r\theta_s)^3\}$$

$$\nabla.\hat{n}_i = N^{-3}\{-h_{ss}(1 - r\theta_s) - rh_s\theta_{ss} - 2\theta_s h_s^2 - \theta_s(1 - r\theta_s)^2\}_{r=h}$$

Finally:

$$k_i = -\nabla.\hat{n}_i = \frac{(\theta_s(1 - h\theta_s)^2 + h_{ss}(1 - h\theta_s) + 2h_s^2\theta_s + hh_s\theta_{ss})}{\{(1 - h\theta_s)^2 + h_s^2\}^{3/2}} \tag{A.17}$$

### *A.2 Non-isothermal flow of a liquid film on horizontal cylinder*

*By B.Reisfeld S.G. Bankoff*

The main reason that this paper is interesting to this thesis is that they are using polar coordinate system, which can be assumed as a special example of normal-tangential coordinate system, this gives us the opportunity of checking the interface conditions. This paper focuses on thin films under the influence of gravity, capillary (due to surface tension forces), thermocapillary (due to the effect of gradients in surface tension) and intermolecular forces (van der Waals forces) on a horizontal cylinder. Analytical solutions are presented first followed by numerical simulations. In the analytical part they derive the evolution equations for interface shapes as a function of azimuthal angle. This Appendix focuses on the interface conditions involving the normal component of the stress tensor. All the other equations and boundary conditions are exactly the same as derived equations in this thesis neglecting gravity, Marangoni and van der Waals effects. We have derived their equation in detail here:

*Coordinate transform*

$$\xi = r - R$$

$$\vec{r} = (\xi + R)\hat{e}_r \qquad r = \xi + R$$

where $\xi = 0$ represents the cylinder surface and $\xi = h(\theta, t)$ represents the gas/liquid interface. The zero stress boundary condition at the top interface in general coordinates can be written as following:

$$\hat{n}.T.\hat{n} = 2H\sigma \qquad H = \frac{1}{2}\nabla.\hat{n} \tag{A.18}$$

*A.2.1 Normal Vector at the top interface*

$$\hat{e}_r = \sin\theta\hat{i} + \cos\theta\hat{j} \qquad \hat{e}_\theta = \cos\theta\hat{i} - \sin\theta\hat{j} \qquad \frac{\partial\hat{e}_r}{\partial\theta} = \hat{e}_\theta$$

$$s = r\theta \qquad \frac{\partial()}{\partial s} = \frac{\partial()}{\partial\theta}\frac{\partial\theta}{\partial s} = \frac{1}{r}\frac{\partial()}{\partial\theta}$$

$$\frac{\partial\vec{r}}{\partial s} = \frac{h_\theta}{r}\hat{e}_r + \frac{h+R}{r}\hat{e}_\theta = \frac{h_\theta}{r}\hat{e}_r + \hat{e}_\theta \tag{A.19}$$

$$\hat{t} = (\frac{h_\theta}{r}, 1)/N \qquad \hat{n} = (1, -\frac{h_\theta}{r})/N \qquad N = \sqrt{(\frac{h_\theta}{r})^2 + 1} \tag{A.20}$$

*A.2.2 Stress Tensor*

The reference "Fluid Dynamics" by Z.U.A Warsi has been used to generate the equations as a function of $(\xi, \theta)$, which are the two independent variables of the system.

$$h_1 = |\frac{\partial\vec{r}}{\partial\xi}| \qquad h_2 = |\frac{\partial\vec{r}}{\partial\theta}|$$

$$DivA = \frac{1}{h_1 h_2}\{\frac{\partial}{\partial\xi}(h_2 A_1) + \frac{\partial}{\partial\theta}(h_1 A_2)\}$$

Stress tensor components for an incompressible 2D flow are:

$$T_{\xi\xi} = -p + 2\mu(\frac{1}{h_1}\frac{\partial u_1}{\partial\xi} + \frac{u_2}{h_1 h_2}\frac{\partial h_1}{\partial\theta})$$

$$T_{\theta\theta} = -p + 2\mu(\frac{1}{h_2}\frac{\partial u_2}{\partial\theta} + \frac{u_1}{h_1 h_2}\frac{\partial h_2}{\partial\xi})$$

$$T_{\xi\theta} = \mu(\frac{1}{h_1}\frac{\partial u_2}{\partial\xi} + \frac{1}{h_2}\frac{\partial u_1}{\partial\theta} - \frac{u_2}{h_1 h_2}\frac{\partial h_2}{\partial\xi} - \frac{u_1}{h_1 h_2}\frac{\partial h_1}{\partial\theta})$$

The velocity vector is $\vec{u} = u\vec{e_r} + v\vec{e_\theta}$.

$$\frac{\partial}{\partial\xi}(u(\xi+R)) + \frac{\partial v}{\partial\theta} = u_\xi(\xi+R) + u + v_\theta = 0 \tag{A.21}$$

$$T_{\xi\xi} = -p + 2\mu(u_\xi) \tag{A.22}$$

$$T_{\theta\theta} = -p + 2\mu(\frac{v_\theta}{\xi + R} + \frac{u}{\xi + R}) = -p - 2\mu u_\xi \tag{A.23}$$

$$T_{\xi\theta} = \mu(v_\xi + \frac{u_\theta}{\xi + R} - \frac{v}{\xi + R}) \tag{A.24}$$

Matrix multiplication leads to:

$$\hat{n}.T.\hat{n} = \{-P + 2\mu u_\xi - \frac{2\mu h_\theta}{\xi + R}(v_\xi + \frac{u_\theta}{\xi + R} - \frac{v}{\xi + R}) - P\frac{h_\theta^2}{(\xi + R)^2} - 2\mu\frac{h_\theta^2}{(\xi + R)^2}u_\xi\}N^{-2}$$

$$= -P + 2\mu\{(1 - \frac{h_\theta^2}{(\xi + R)^2})u_\xi - \frac{h_\theta}{\xi + R}(v_\xi - \frac{v}{\xi + R}) - \frac{h_\theta}{\xi + R}(\frac{u_\theta}{\xi + R})\}N^{-2}$$

To make the result similar to the Reisfeld and Bankoff form we define:

$$u_\xi = -\frac{u + v_\theta}{\xi + R} \qquad (v_\xi - \frac{v}{\xi + R}) = (\xi + R)(\frac{v}{\xi + R})_\xi.$$

The final form of $\hat{n}.T.\hat{n}$ is:

$$-p + \frac{2\mu}{\xi + R}\{(\frac{h_\theta^2}{(\xi + R)^2} - 1)(u + v_\theta) - h_\theta(\xi + R)(\frac{v}{\xi + R})_\xi - h_\theta(\frac{u_\theta}{\xi + R})\}.N^{-2} \tag{A.25}$$

where

$$N = \sqrt{\frac{h_\theta^2}{(\xi + R)^2} + 1} \tag{A.26}$$

*A.2.3 Curvature calculation :* $2H = \nabla.\hat{n}$

Again by using the definition of the divergence the curvature follows:

$$\nabla.\hat{n} = \frac{1}{\xi + R}\{\frac{\partial}{\partial\xi}(\frac{\xi + R}{N}) + \frac{1}{\xi + R}\frac{\partial}{\partial\theta}(\frac{-h_\theta}{N})\}$$

$$N_\xi = \frac{-h_\theta^2}{(\xi + R)^3}N^{-1} \qquad N_\theta = \frac{h_\theta h_{\theta\theta}}{(\xi + R)^2}$$

$$\nabla.\hat{n} = \frac{1}{\xi + R}\{(N - (\xi + R)N_\xi) - \frac{1}{(\xi + R)}(h_{\theta\theta}N - h_\theta N_\theta)\}N^{-2}$$

$$\nabla.\hat{n} = \frac{1}{\xi + R}N^{-1} + \frac{h_\theta^2}{(\xi + R)^3}N^{-3} - \frac{h_{\theta\theta}}{(\xi + R)^2} + \frac{h_\theta^2 h_{\theta\theta}}{(\xi + R)^4}N^{-3} \tag{A.27}$$

To compare with Equation 3.12 in the Reisfeld and Bankoff paper, the factor of $N^{-3}$ needs to be taken from the right hand side and both sides are multiplied by $-1$. Thus $\hat{n}.T.\hat{n} = 2H\sigma$ and:

$$\begin{aligned} p - \frac{2\mu}{\xi + R}\{(\frac{h_\theta^2}{(\xi + R)^2} - 1)(u + v_\theta) - h_\theta(\xi + R)(\frac{v}{\xi + R})_\xi - h_\theta(\frac{u_\theta}{\xi + R})\}.N^{-2} \\ = -\sigma N^{-3}(\frac{1}{\xi + R}N^2 - \frac{h_{\theta\theta}}{(\xi + R)^2}N^2 + \frac{h_\theta^2}{(\xi + R)^3} + \frac{h_\theta^2 h_{\theta\theta}}{(\xi + R)^4}) \end{aligned} \tag{A.28}$$

*A.2.4 Scaling*

$$\zeta = \frac{\xi}{d_o} \qquad P = \frac{p}{P_o} \qquad U = \frac{u}{u_o} \qquad V = \frac{V}{v_o} \qquad H = \frac{h}{d_o}$$

$$u_o = \frac{\nu}{R} \qquad v_o = \frac{\nu}{d_o} \qquad \frac{d_o}{R} = \epsilon \qquad \frac{u_o}{v_o} = \frac{d_o}{R} = \epsilon \qquad p_o = \frac{\rho\nu^2 R}{d_o^3} = \frac{\mu v_o}{d_o \epsilon}$$

where $d_o$ is the initial film thickness and $R$ is the cylinder radius. The following is the term by term scaling process:

$$N_\epsilon = \{\frac{(Hd_o)_\theta^2}{(\zeta d_o + R)^2} + 1\}^{1/2} = \{\frac{(H^2)_\theta d_o^2}{R^2(\zeta d_o/R + 1)^2} + 1\}^{1/2} = \{\frac{\epsilon^2 H_\theta^2}{(1 + \epsilon\zeta)^2} + 1\}^{1/2}$$

$$\frac{2\mu}{\xi + R}N^{-2} \Longrightarrow \frac{2\mu}{R(1 + \epsilon\zeta)}N_\epsilon^{-2}$$

$$u + v_\theta \Longrightarrow u_o U + V_\theta v_o = v_o(\epsilon U + V_\theta)$$

$$h_\theta(\xi + R)(\frac{v}{\xi + R})_\xi \Longrightarrow H_\theta d_o R(1 + \epsilon\zeta)\frac{1}{d_o}(\frac{V v_o}{R(1 + \epsilon\zeta)})_\zeta = v_o H_\theta(1 + \epsilon\zeta)(\frac{V}{1 + \epsilon\zeta})_\zeta$$

$$h_\theta\frac{u_\theta}{\xi + R} \Longrightarrow \frac{H_\theta d_o U_\theta u_o}{R(1 + \epsilon\zeta)} = v_o\frac{\epsilon^2 H_\theta U_\theta}{1 + \epsilon\zeta}$$

The terms on the right hand side are scaled:

$$P\frac{\mu v_o}{d_o\epsilon} - \frac{2\mu v_o}{R(1+\epsilon\zeta)}N_\epsilon^{-2}\{(\frac{\epsilon^2 H_\theta^2}{(1+\epsilon\zeta)^2} - 1)(\epsilon U + V_\theta) - H_\theta(1+\epsilon\zeta)(\frac{V}{1+\epsilon\zeta})_\zeta - \epsilon^2 H_\theta\frac{U_\theta}{1+\epsilon\zeta}\}$$

$$= -\frac{\sigma}{R}N_\epsilon^{-3}\{\frac{1}{1+\epsilon\zeta}N_\epsilon^2 - \frac{\epsilon H_{\theta\theta}}{(1+\epsilon\zeta)^2}N_\epsilon^2 + \frac{\epsilon^2 H_\theta^2}{(1+\epsilon\zeta)^3} + \frac{\epsilon^3 H_\theta^2 H_{\theta\theta}}{(1+\epsilon\zeta)^4}\}$$

Both sides are divided by $\mu v_o/(d_o\epsilon)$ and defining the capillary number as $Ca = (\mu v_o)/\sigma$ gives:

$$P - \frac{2\epsilon^2}{(1+\epsilon\zeta)}N_\epsilon^{-2}\{(\frac{\epsilon^2 H_\theta^2}{(1+\epsilon\zeta)^2} - 1)(\epsilon U + V_\theta) - H_\theta(1+\epsilon\zeta)(\frac{V}{1+\epsilon\zeta})_\zeta - \epsilon^2 H_\theta\frac{U_\theta}{1+\epsilon\zeta}\}$$

$$= -Ca^{-1}\epsilon^3 N_\epsilon^{-3}\{\frac{1}{\epsilon(1+\epsilon\zeta)}N_\epsilon^2 - \frac{H_{\theta\theta}}{(1+\epsilon\zeta)^2}N_\epsilon^2 + \frac{\epsilon H_\theta^2}{(1+\epsilon\zeta)^3} + \frac{\epsilon^2 H_\theta^2 H_{\theta\theta}}{(1+\epsilon\zeta)^4}\}$$

Although there are some differences in the LHS there are no differences in the RHS of the two results. Both end up giving us same $O(1)$ equations

$$P = -\tilde{C}^{-1}(\frac{1}{\epsilon}(1-\epsilon\zeta) - H_{\theta\theta}) = -\tilde{C}^{-1}(\epsilon^{-1} - \zeta - H_{\theta\theta})$$

$$\zeta = H$$

$$P = -\tilde{C}^{-1}(\epsilon^{-1} - H - H_{\theta\theta}) \tag{A.30}$$

where

$$Ca^{-1} \sim O(\epsilon^{-3}) \Longrightarrow \tilde{C}^{-1} = Ca^{-1}\epsilon^3 \sim O(1)$$

and

$$\epsilon \to 0 \Longrightarrow N_\epsilon \to 1$$

Their pressure profile is the same as the one that has been derived in this thesis if the dimensionless curvature is set to the appropriate value unity, and noting that $\theta$ in their equations can be replaced by scaled arc-length ($S = \theta$).

# BIBLIOGRAPHY

[1] George V. Franks Graeme J. Jameson Timothy N. Hunter, Robert J. Pugh. The role of particles in stabilising foams and emulsions. *Advances in Colloid and Interface Science*, 137:57–81, 2008.

[2] Pierre-Gilles de Gennes Franoise Brochard-Wyart David Qur. *Capillarity and Wetting Phenomena*. Springer, 2002.

[3] H. Bouasse. *Capillarit - Phnomnes superficiels ( Capillarity and surface phenomena)*. Paris: Delagrave, 1924.

[4] Stephen H. Davis. *PERSPECTIVE IN FLUID DYNAMICS ( A Collective Introduction to Current Research)*. Cambridge university press.

[5] L. N. Brush and S. H. Davis. A new law of thinning in foam dynamics. *Fluid Mech.*, 534:227–236, 2005.

[6] L. N. Brush and S. M. ROPER. The thinning of lamellae in surfactant-free foams with non-newtonian liquid phase. *Fluid Mech.*, 616:235–262, 2008.

[7] T. G. Myers. Application of non-newtonian models to thin film flow. *PHYSICAL REVIEW E*, 72, 2005.

[8] Dimitri Vaynbalt & John R. Lister & Thomas P. Witelski. Rupture of thin viscous films by van der waals forces: Evolution and self similarity. *PHYSICAL OF FLUID*, 13, 2001.

[9] Anthony M. Anderson & Lucien N. Brush & Stephen H. Davis. Foam mechanics: spontaneos rupture of thinning liquid films with plateau borders. *Fluid Mech.*, 2010.

[10] Z. U. A Warsi. *Fluid dynamics: Theoretical and Computational Approaches*. CRC Press, Inc, 1992.

[11] P. D. Howell. The draining of a two-dimensional bubble. *Engineering Mathematics*, 35:251–272, 1999.

[12] B. Reisfeld & S. G. Bankoff. Non-isothermal flow of a liquid film on a horizontal cylinder. *Fluid Mech.*, 236:167–196, 1991.

[13] M. Beerman and L. N. Brush. Oscillatory instability and rupture in a thin melt film on its crystal subject to freezing and melting. *Fluid Mech.*, 586:423–448, 2007.

[14] E. Ruckenstein and K Jain, R. Spontaneous rupture of thin liquid films. *Chem. Soc. Faraday Trans*, 270:132–137, 1974.

[15] Dussan V. E. B and S. H Davis. On the motion of a fluid-fluid interface along a solid surface. *Fl*, 65:95–97, 1974.

[16] P. D. Howell. *Extensional Thin layer flows*. PhD thesis, St. Catherines College Oxford, 1994.

[17] R. A. L. & Gruzleski J. E. Anson, J. P. Drew. The surface tension of molten aluminum and ag-si-mg alloy under vacuum and hydrogen atmospheres. *Metall. Matter. Trans*, B30:1027–1032, 1999.

[18] S. H & Hiroshi A. Hur, B. Y. Park. Viscosity and surface tension of al and effects of additional element. *Eco-materials Processing and Design , Mater. Sci Forum*, 439: 51–56, 1989.

[19] P. N Dinsdale, A. T. & Quested. The viscosity of aluminum and its alloys. *Material Sci.*, 39:7221–7228, 1999.

[20] Clint JH Aveyard R, Binks BP. *Adv Colloid Interface Sci*, 46:100–102–503, 2003.

[21] Michael Beerman. *Tranverse Freezing of Thin Liquid Films*. PhD thesis, University of Washington, 2007.

[22] Dickinson E. An introduction to food colloids. *Oxford university press*, 1992.

[23] Speight JG. The chemistry and technology of petroleum. *Ma*, 1991.

[24] Lissant KJ. Emulsions and emulsion chemistry part 1. *Marcer Dekker Inc*, 6, 1974.

[25] Khan SA. Prud'homme RK. Foams-theory, measurements and application. *Marcer Dekker Inc*, 1996.

[26] Sharma MM Tambe DE. *Colloids Interface Sci*, 53:157–244, 1993.